Performance of a Saturation-Based Dissipation-Rate Source Term in Modeling the Fetch-Limited Evolution of Wind Waves

JOSE HENRIQUE G. M. ALVES AND MICHAEL L. BANNER

School of Mathematics, The University of New South Wales, Sydney, New South Wales, Australia

(Manuscript received 7 August 2001, in final form 29 October 2002)

ABSTRACT

A new formulation of the spectral dissipation source term S_{ds} for wind-wave modeling applications is investigated. This new form of S_{ds} is based on a threshold behavior of deep-water wave-breaking onset associated with nonlinear wave-group modulation. It is expressed in terms of the azimuth-integrated spectral saturation, resulting in a nonlinear dependence of dissipation rates on the local wave spectrum. Validation of the saturation-based S_{ds} is made against wave field parameters derived from observations of fetch-limited wind-wave evolution. Simulations of fetch-limited growth are made with a numerical model featuring an exact nonlinear form of the wave–wave-interactions source term S_{nl}. For reference, the performance of this saturation-based S_{ds} is compared with the performance of the wave-dissipation source-term parameterization prescribed for the Wave Modeling Project (WAM) wind-wave model. Calculations of integral spectral parameters using the saturation-based model for S_{ds} agree closely with fetch-limited observations. It is also shown that the saturation-based S_{ds} can be readily adjusted to accommodate several commonly used parameterizations of the wind input source term S_{in}. Also, this new form of S_{ds} provides greater flexibility in controlling the shape of the wave spectrum in the short gravity-wave region.

1. Introduction

Most wind-wave models presently used in operational sea-state forecasting are based on the numerical solution of the spectral energy balance equation,

$$\frac{\partial F(k,\,\theta)}{\partial t} + \nabla \cdot \mathbf{c}_g F(k,\,\theta) = S_{in} + S_{nl} + S_{ds}. \quad (1)$$

In deep water, Eq. (1) describes the time evolution of the wave energy density spectrum $F(k,\,\theta)$ as the result of spatial propagation of spectral components with group velocity $\mathbf{c}_g$, wavenumber k, direction θ, and forcing determined by three physical processes: wind input, resonant nonlinear wave–wave interactions, and energy dissipation, with S_{in}, S_{nl}, and S_{ds} representing the corresponding spectral source terms. For wave modeling, extensive analytical and observational efforts have led to the development of acceptable parameterizations of S_{in} and S_{nl}.

For wind-driven seas, wave breaking is believed to be the dominant dissipative process contributing to S_{ds}, possibly augmented by other mechanisms such as wave–turbulence interaction. However, because of the extreme difficulties involved in observing wave breaking and wave–turbulence interactions in the field, dissipation is the least understood physical process associated with the evolution of wind waves. As a consequence, present state-of-the-art operational wind-wave models such as Wave Modeling Project (WAM; Komen et al. 1994), Simulating Waves Near Shore (SWAN; Booij et al. 1999), and Wave Height, Water Depth, and Current Hindcasting (WAVEWATCH III; Tolman 1999) compute S_{ds} through parametric functions based on general theoretical arguments.

Despite the difficulties, recent developments have contributed new insight toward understanding and modeling wave breaking and have motivated the saturation-based form of S_{ds} investigated in this paper. Our investigation of S_{ds} is based on simulations of fetch-limited wind-wave evolution using a research model featuring an exact nonlinear form of S_{nl}. This approach is a sequel to the study of Banner and Young (1994, henceforth BY94) on the form of S_{ds} used in the WAM Cycle-3 model.

The computations of fetch-limited evolution reported in BY94 using the WAM Cycle-3 quasi-linear form of S_{ds} revealed several deficiencies attributed to the specification of this dissipation source term. Their analysis showed that model results did not reproduce optimally the power-law fetch dependence of total energy and peak frequency found in field observations. BY94 also found that model spectra did not reproduce well the observed two-dimensional properties of fetch-limited spectra, including the directional spreading at the spectral peak and the high-wavenumber tail energy levels,

Corresponding author address: Prof. Michael L. Banner, School of Mathematics, The University of New South Wales, 2052 Sydney, Australia.
E-mail: m.banner@unsw.edu.au

as well as their equilibrium range power-law dependence on the wavenumber.

The motivation for the present study was to investigate a revised form of S_{ds} to address these perceived deficiencies, drawing on the recent developments in understanding wave breaking reported in the literature. We believe that this approach can provide a more physically based framework for improving parameterizations of S_{ds} and can allow for refinements in wave-model prediction of quantities related to wave breaking, including the estimation of wave-breaking-mediated fluxes at the air–sea interface.

This paper is structured as follows. Section 2 provides a review of the relevant modeling and observational background. Section 3 provides an overview of the empirical and conceptual framework that supports a saturation-based S_{ds}. Section 4 describes the numerical model, the validation strategy, and the diagnostic parameters used throughout our study. Section 5 gives an update to the study of BY94 through assessing the benefits to model performance of recent changes in the dissipation source term used in WAM model. Results of the simulations made with our saturation-based form of S_{ds} are reported in section 6. Section 7 summarizes the major results of our investigation and our recommendations for future research.

2. Modeling and observational framework

The saturation-based form of S_{ds} investigated in this study has its origins in a number of previous studies that highlight the strong underlying role in the onset of deep-water wave breaking of nonlinear wave-group dynamics and the associated wave steepness threshold. Early evidence of this connection between wave groups and wave breaking is found in field observations reported in Donelan et al. (1972) and Holthuijsen and Herbers (1986). Subsequent numerical model investigations of two-dimensional nonlinear wave-group evolution based on the exact Euler equations, pioneered by Dold and Peregrine (1986), complement these early observational studies. Further confirmation is provided by Rapp and Melville (1990), who reported that modulating wave groups observed in the laboratory evolved to breaking whenever a measure of the *initial* group steepness exceeded a threshold value. This threshold was dependent on the number of waves in the modulating group, as reported in Dold and Peregrine (1986). The very recent study by Song and Banner (2002) reported a breaking threshold that is independent of initial group structure and size. Their proposed threshold is based on an intrinsic growth-rate parameter that quantifies the energy flux rate within modulating wave groups.

Field support for this breaking-threshold behavior was reported recently by Banner et al. (2000, henceforth BBY) in their study of the breaking probability of dominant sea waves. Their results based on observations made in a very wide range of sea-state conditions indicated a strong correlation between the wave-breaking probability and a significant wave steepness parameter. Further, this correlation showed that a threshold behavior was operative in controlling the breaking of dominant waves. The results of BBY also suggested that the threshold behavior observed for the spectral peak waves might extend to the shorter waves within the spectral tail. However, for these shorter waves, the probability and/or intensity of breaking events due to nonlinear wave-group modulation might be influenced by their stronger directionality, as reported in recent laboratory studies such as She et al. (1997) and Nepf et al. (1998).

These studies highlighted the primary role of nonlinear wave-group modulation in the onset of breaking of deep-water wind waves, with a threshold behavior based on a representative mean wave steepness. This provided the basis for the development of the form of S_{ds} proposed in this study, which embodies the wave steepness locally in terms of the spectral saturation. Within this conceptual framework, the parameterization for S_{ds} needs to reflect how these dissipation rates are distributed spectrally. The viewpoint adopted here is a proposed refinement of the form of S_{ds} described in Komen et al. (1994). Depending on the stage of spectral development (wave age), wave breaking can occur at any spectral scale, including the spectral peak, and the associated energy dissipation rate S_{ds} removes energy from that scale. A major contribution to the dissipation rate at a given spectral scale results from the work done by the breaking region in reducing the excess wave orbital velocity field on the scale of the actively breaking wave.

This viewpoint is also supported by an analysis of field data by Donelan (1996). Based on energy fluxes rather than changes in spectral shape, Donelan (1996) argues that at the spectral peak the major flux balance is between wind input and dissipation. This requires a dissipation source term that is strongly nonlinear in the wave spectrum, with relatively high dissipation rates at the spectral peak for young wind seas that decrease progressively toward full development. In the formulation of a physically based form of S_{ds}, there is also the need to parameterize other known dissipative mechanisms such as background dissipation by subsurface turbulence and short-wave damping through the passage of modulating longer waves. We note also that wind input is not necessary for wave breaking to occur, because self-modulating unforced nonlinear wave groups can also evolve with breaking provided that the mean wave steepness is sufficiently large. This situation could arise for waves traveling against or faster than the wind.

We note that the above approach is in contrast with the wave turbulence cascade viewpoint (e.g., Zakharov and Filonenko 1967; Kitaigorodskii 1983) in which the dissipation is envisaged to occur locally only in the high-wavenumber tail region. There have also been efforts to elucidate the spectral implications of wave breaking in a number of recent laboratory studies that involve focused wave packets (e.g., Rapp and Melville

1990; Meza et al. 2000) and modulated wave groups (e.g., Tulin and Waseda 1999), but their findings are not considered to be conclusive. From changes in the spectral signatures of transient wave groups before and after breaking, Meza et al. (2000) argued that dissipation rates were concentrated mainly in the higher frequencies, with little apparent evidence of energy loss around the spectral peak. In contrast, Tulin and Waseda (1999) found that wave breaking due to nonlinear wave-group modulation can result in significant changes of energy density levels at the initial spectral peak. Thus, in the context of field conditions that involve evolution under wind input and weakly nonlinear four-wave interactions, it is even harder to draw any definite conclusions from these laboratory studies. Owing to the difficulty in making direct observations of S_{ds} either in the field or in the laboratory, the issue of the spectral distribution of the wave energy dissipation rate remains a significant challenge.

3. Parameterizations of S_{ds}

A major goal of operational wind-wave forecasting is to determine a simple parameterization in a phase-averaged (spectral) model that reflects the issues outlined in the previous section, including the breaking threshold behavior due to nonlinear wave-group modulation observed in the laboratory and at sea. A purely empirical parameterization of spectral dissipation rates, however, cannot yet be made because of the lack of appropriate dissipation-rate data. On the other hand, parameterizations developed directly from the results of fully nonlinear free-surface model computations are based on variables that depend on the local structure of the wave group—for example, the energy convergence rate at the modulating wave-group maxima used in Song and Banner (2002). Such variables, however, are inaccessible in spectral wave models.

To make progress, we introduce a form for S_{ds} that uses a surrogate stochastic parameter that reflects the underlying wave-group hydrodynamics described above. This parameter needs to provide a wide dynamic range of dissipation rates within the spectral peak region, with high levels of dissipation in strongly forced situations and only residual dissipation rates in mature or fully developed conditions. It also needs to provide a substantial dissipation-rate level within the high-frequency spectral range (the spectral tail), with a relatively small dynamic range of variation during all wind-sea development stages. In addition, the formulation of S_{ds} has to allow enough flexibility to include parameters that represent the effect of other contributions to spectral dissipation rates, including viscous decay and fluxes from the wave field through wave–turbulence interactions, as highlighted by Thais and Magnaudet (1996) and Drennan et al. (1997), among others.

a. Quasi-linear form of S_{ds}

The requirements outlined above challenge the concept introduced by Hasselmann (1974) of a quasi-linear dissipation source term, such as the form of S_{ds} used in WAM. This parameterization of S_{ds}, described in Komen et al. (1994), is given by

$$S_{ds}(k, \theta) = -C_{ds}\left(\frac{\hat{\alpha}}{\hat{\alpha}_{PM}}\right)^{m}\left[(1-\delta)\frac{k}{\overline{k}} + \delta\left(\frac{k}{\overline{k}}\right)^{2}\right]^{n/2}\overline{\omega}F(k, \theta), \quad (2)$$

where $\alpha = E_{tot}\overline{k}^{2}$ is an integral steepness parameter, $\hat{\alpha}_{PM} = 4.57 \times 10^{-3}$ is the integrated steepness of a fully developed Pierson–Moskowitz spectrum (Pierson and Moskowitz 1964), $\overline{k}$ is the mean wavenumber, $\overline{\omega}$ is the mean angular frequency, θ is the wave direction, and δ is a weighting factor that controls the magnitude of linear and quadratic functions of the ratio $k/\overline{k}$. Here E_{tot} is the total wave energy obtained by integrating the directional wavenumber spectrum $F(k, \theta)$.

The default WAM Cycle-3 setup has $\delta = 0$, $m = 2$, and $n = 2$; the WAM Cycle-4 model has $\delta = 0.5$, $m = 2$, and $n = 1$. For simplicity, reference to Eq. (2) will be made explicitly or using the symbol S_{ds}^{W}. Specific reference to either forms used in the WAM Cycle-3 or Cycle-4 configurations will be made using S_{ds}^{W3} or S_{ds}^{W4}, respectively.

At the time the quasi-linear S_{ds} model defined by Eq. (2) was formulated based on Hasselmann (1974), the importance of wave groupiness and hence the underlying role of a finite spectral bandwidth in the breaking onset process was not recognized. Thus the argument of a limiting narrowband spectrum justifying this quasi-linear form and used to preclude the development of other forms of S_{ds} nonlinearly dependent on the local value of the energy density spectrum $F(k, \theta)$ is no longer considered to be valid. Further discussion on this topic is provided by Donelan and Yuan (1994).

b. A saturation-based S_{ds}

In view of the ongoing issues and recent developments outlined in section 2, an alternative form of S_{ds} is proposed that is consistent with a threshold behavior of the breaking onset of deep-water waves, as follows:

$$S_{ds}(k, \theta) = -C_{ds}\left[\frac{B(k)}{B_r}\right]^{p/2}(E_{tot}k_p^2)^{m}\left(\frac{k}{\overline{k}}\right)^{n}\omega F(k, \theta), \quad (3)$$

where $B(k) = k^4\mathcal{F}(k)$ is a local saturation parameter defined in terms of the azimuth-integrated wavenumber spectrum $\mathcal{F}(k)$ [see Eq. (4) below], $E_{tot}k_p^2$ is an integral spectral steepness parameter and k_p is the peak wavenumber. The threshold saturation level B_r, the coefficient C_{ds}, and the exponents m and n are all constants that need to be determined numerically to allow match-

ing the computed spectral quantities to observations. A detailed description of these variables and of their relative importance and contribution to Eq. (3) is presented below.

Our investigation provides a thorough assessment of this saturation-based form of S_{ds} (henceforth S_{ds}^{B}) through numerical simulations of fetch-limited wind-wave evolution. It is noteworthy that the general structure of Eq. (3) is consistent with other nonlinear forms of S_{ds} previously suggested by Phillips (1984, 1985), Donelan and Pierson (1987), and Donelan (1996), premised on dynamical arguments different from those that motivated our proposed formulation. For a review of these other conceptual forms for S_{ds}, the reader is referred to Donelan and Yuan (1994). Other recent efforts to improve wave-model performance have been made by Tolman and Chalikov (1996) and Schneggenburger et al. (2000), using parameterizations of S_{ds} that also depend nonlinearly on the wave spectrum.

1) CONCEPTUAL BASIS

In the ocean, the stochastic nature of wave-group lengths and geometries precludes specifying any initial steepness condition, as is the practice in wave-tank experiments and numerical calculations of wave train evolution. Because the physics of wave breaking due to nonlinear wave-group modulation cannot be incorporated directly into spectral wave models, as discussed previously, we introduced a spectral steepness measure derived from the local wave energy density spectrum that reflects the nonlinearity of the wave field and provides the basis for a breaking threshold variable.

Our search for a suitable bandwidth-independent measure of spectral steepness led to a nondimensional spectral saturation parameter $B(k) = k^4\mathcal{F}(k)$, where the azimuth-integrated wavenumber spectrum is defined by

$$\mathcal{F}(k) = \int_{-\pi}^{\pi} F(k, \theta)\, d\theta. \tag{4}$$

This azimuth-integrated saturation parameter $B(k)$, introduced more generally as a function of the local wavenumber spectrum in the form $B(k, \theta) = k^4F(k, \theta)$ by Phillips (1984, 1985), is also conveniently related to the mean squared slope:

$$\begin{aligned} \text{mss} &= \int\int k^4F(k, \theta)\, d(\ln k)\, d\theta \\ &= \int k^4\mathcal{F}(k)\, d(\ln k), \end{aligned} \tag{5}$$

where $d(\ln k) = dk/k$ is the relative wavenumber bandwidth.

Although many variants of a saturation-based S_{ds} are possible, the form defined by Eq. (3) reflects the general findings of BBY, addressing the need for a threshold behavior by using a nonlinear dependence on the ratio of the azimuth-integrated saturation $B(k)$ to a reference saturation threshold level B_r. Further, because the overall dissipation rate at a given k is proportional to the product of the breaking probability and the breaking strength, Eq. (3) also implies a threshold behavior for the breaking strength.

2) OTHER CONTRIBUTIONS

Although a primary threshold dependence on the local spectral steepness in terms of a saturation ratio underpins our proposed S_{ds} formulation, we found that additional spectral dissipation at the high-wavenumber spectral range was needed to provide robust results over the wide range of wave ages encountered at sea. These additional dissipation levels were provided by a weighting function, which may be regarded as reflecting incompletely understood dissipation effects that involve the interaction between small-scale and large-scale wave components. Such physical processes include the rapid attenuation of short waves in the wake of larger breakers (Banner et al. 1989) and the mechanism underlying the attenuation of shorter wind waves resulting from the passage of long waves (Mitsuyasu 1966; Phillips and Banner 1974; Donelan 1984; Chu et al. 1992; Chen and Belcher 2000).

Dissipation rates may also be enhanced through the interaction between waves and general background turbulence. Early experimental evidence of this process was given by Green et al. (1972), who measured wave dissipation due to turbulence generated by an oscillating submerged grid in the laboratory and found that decay rates were proportional to the wave steepness. Kolaini and Tulin (1995) indicate that large-scale background turbulence generated by breaking waves induces changes in the breaking severity and heights of succeeding waves. This effect was also observed in lakes (Agrawal et al. 1992) and in the open ocean (Gemmrich and Farmer 1999). A review of other experimental studies on this topic is also provided in Drennan et al. (1997).

Although observational evidence does not provide a clear understanding of the mechanisms causing enhanced wave energy dissipation due to long-wave–short-wave and wave–turbulence interactions, there seems to be a general consensus that these two mechanisms should be included in empirical formulas used to compute spectral dissipation rates. To allow an assessment of the sensitivity of model results to including these effects, we assumed that these mechanisms were represented collectively through a dependence of S_{ds} on the integrated spectral steepness parameter $E_{tot}k_p^2$, where k_p is the spectral peak wavenumber, and a weighting function $(k/\overline{k})^n$ proportional to the local wavenumber k relative to the mean wavenumber $\overline{k}$, operative for $k > \overline{k}$.

3) ADDITIONAL CONSTRAINTS

Based on these considerations, the combination of parameters representing dissipative processes led to the general function describing spectral dissipation rates given by Eq. (3). To ensure the consistency of this general saturation-based form of S_{ds} with observations reported in Rapp and Melville (1990) and BBY, an additional constraint was imposed. These two studies suggest that the breaking-wave contribution to S_{ds} should become negligible whenever the chosen threshold breaking parameter falls below a critical level. In our case, this would happen whenever $B(k) < B_r$. However, because it is desirable that other dissipative processes (e.g., straining of shorter waves and wave–turbulence interactions) remain active as background sources of energy loss, the term $[B(k)/B_r]^{p/2}$ cannot vanish when $B(k) < B_r$.

For convenience, we assumed that the term $[B(k)/B_r]^{p/2}$ asymptotically approaches unity whenever $B(k) < B_r$. In this way, the remaining terms will set the background dissipation rate of spectral components with reduced steepness, such as swell and waves traveling faster than or opposing the local wind speed vector or in the absence of wind. This is achieved by defining the exponent p as a function of the ratio $B(k)/B_r$, as follows:

$$p = \frac{p_0}{2} + \frac{p_0}{2}\tanh\left\langle 10\left\{\left[\frac{B(k)}{B_r}\right]^{1/2} - 1\right\}\right\rangle, \qquad (6)$$

where p_0 is a constant that needs to be determined numerically. Equation (6) defines p as a function that is equal to 0 when $B(k) < B_r$ and equal to p_0 otherwise.

c. Quasi-linear versus saturation-based S_{ds}

The general structure of the saturation-based S_{ds}, Eq. (3), resembles that of the quasi-linear form, Eq. (2), in the sense that both may be reduced to the general form $S_{ds}(k, \theta) = \gamma F(k, \theta)$. However, in the saturation-based form S_{ds}^B, γ is a function of the wavenumber k and depends nonlinearly on the steepness of the local wavenumber spectrum. This dependence leads to $\gamma(k) \propto \mathcal{F}(k)^{p/2}(k/\bar{k})^n$ at any particular stage of wave development. In contrast, S_{ds}^W has $\gamma \propto (k/\bar{k})^n$ at any given wavenumber, because it is proportional only to the integrated spectral energy E_{tot}, which is independent of the wavenumber k and is a constant at any particular wave development stage.

These conceptual distinctions between Eqs. (2) and (3) for S_{ds} produce significant differences in practical terms, as shown in Fig. 1. This figure indicates the modest dynamic range of dissipation rates near the spectral peak relative to the spectral tail region in the S_{ds}^W formulation, as the seas develop from young to old. On the other hand, the S_{ds}^B model provides a larger relative peak–tail dynamic range. In the latter behavior, the high breaking probabilities of dominant waves for young wind seas reduce progressively and become relatively small near full development, reflecting the empirical behavior suggested by results summarized in Fig. 2 of BBY. This large dynamic range of spectral peak dissipation rates is also prescribed by the form of S_{ds} proposed by Tolman and Chalikov (1996).

4. Numerical modeling approach

When spatially homogeneous and steady winds blow perpendicularly offshore from a straight coastline, the initial downwind evolution of the wave field will be governed by the one-dimensional form of the energy balance equation [Eq. (1)], as follows:

$$\left(\frac{\partial}{\partial t} + c_g \cos\theta \frac{\partial}{\partial x}\right) F(k, \theta) = S_{in} + S_{nl} + S_{ds}, \qquad (7)$$

where x is the spatial dimension aligned with the wind direction and $c_g = |\mathbf{c}_g|$.

The wave field will become fetch limited if the homogeneous, steady wind field persists over a sufficiently long period. In this case, Eq. (7) may be simplified by eliminating the unsteady term $\partial F(k, \theta)/\partial t$. The propagation in space of the resulting steady-state equation may be solved numerically by using a simple two-point grid, where the spatial derivatives are discretized via a first-order forward-difference scheme (Komen et al. 1984; Young and Van Vledder 1993; BY94). This numerical approach leads to a singularity appearing in the numerical solution for spectral components propagating at angles near 90° and unstable behavior in the high-wavenumber range (Alves 2000, henceforth A00).

In this study, a numerical scheme that retains the unsteady term $\partial F(k, \theta)/\partial t$ was used to eliminate the singularity appearing at $\theta = 90°$, providing a better convergence of model results toward an equilibrium state. This numerical approach was implemented into the research wind-wave model described in Tracy and Resio (1982, henceforth TR82), featuring an exact nonlinear form of S_{nl}, which we used to solve Eq. (7). Following a suggestion made by H. Tolman (1999, personal communication), this numerical scheme implemented in the TR82 code consisted simply of iterating each spatial propagation step of the two-point numerical grid over artificial time steps until convergence to a steady state was reached. Spatial propagation was solved numerically using a first-order forward-difference scheme with a dynamically adjusted spatial step. The chosen numerical approach retaining the unsteady term was particularly important at short fetches, when the wind sea was young and the spectral energy density was concentrated at very short wavelengths. The drawback of retaining the unsteady term was an increase by one order of magnitude in the computational time.

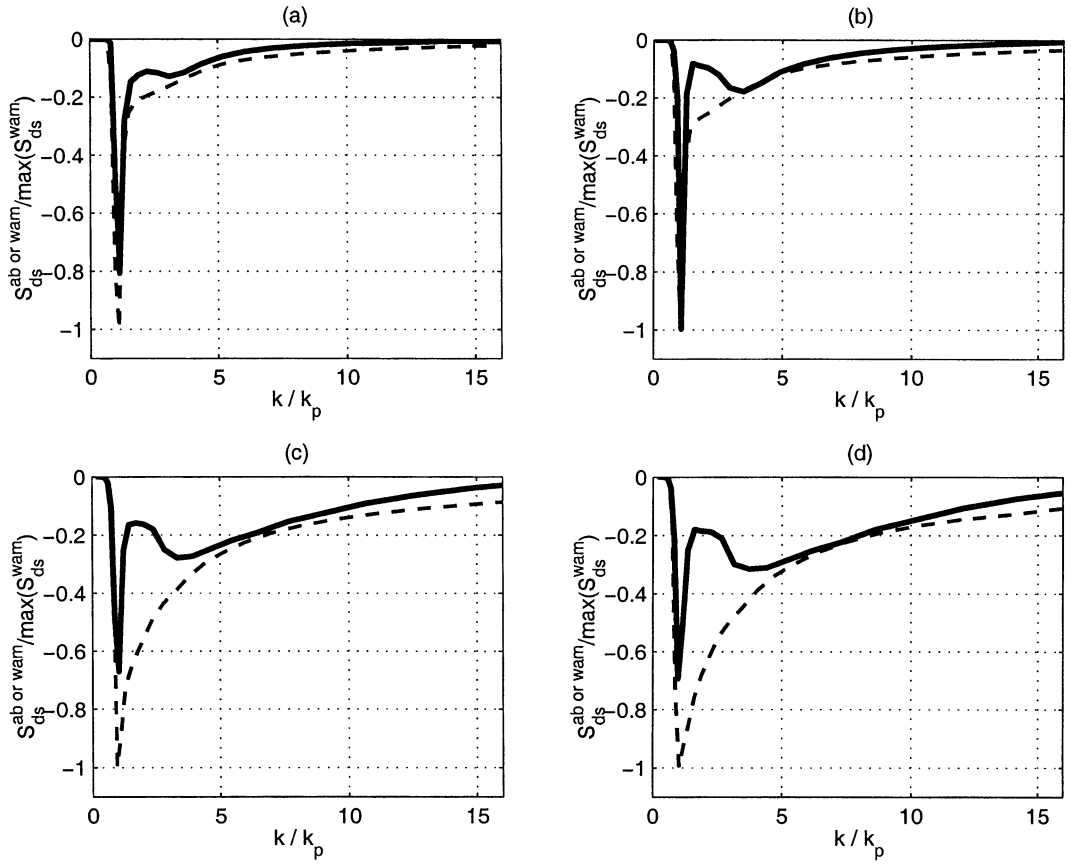

FIG. 1. Spectral dissipation rates estimated with S_{ds}^{B} (continuous lines) and S_{ds}^{W} (broken lines) for (a) young wind seas ($U/c_p = 2.5$), (b) mature wind seas ($U/c_p = 1.5$), (c) waves near full development ($U/c_p = 1$), and (d) fully developed seas ($U/c_p \approx 0.9$). Dissipation rates are normalized by the maximum absolute S_{ds}^{W} level ($\times -1$) at each development stage.

a. Model physics

The TR82 model includes an exact nonlinear algorithm to solve the S_{nl} integral, which evaluates the nonlinear transfer of action density between four interacting wavenumber vectors $\mathbf{k}_1$, $\mathbf{k}_2$, $\mathbf{k}_3$, and $\mathbf{k}_4$. This algorithm is based on the Webb–Resio–Tracy (WRT) method consisting of the exact solution of S_{nl} derived by (Webb 1978) and adapted by TR82. The version of the WRT method used in our study utilizes a discrete wavenumber grid with Δk defined in terms of a geometric progression. According to TR82, this provides a considerable reduction of the computational effort required for the exact solution of S_{nl}. Other properties of the WRT method are discussed in TR82 and BY94.

Following BY94, our numerical experiments initially used the form of S_{in} from Yan (1987) (henceforth S_{in}^{Y}):

$$S_{in}^{Y}(k,\ \theta) = \left\{\left[0.04\left(\frac{u_*}{c}\right)^2 + 0.005\ 44\frac{u_*}{c} + 0.000\ 055\right] \times \cos\theta - 0.000\ 31\right\}\omega F(k,\ \theta). \quad (8)$$

Equation (8) provides estimates of wind input rates that follow the parameterizations of Snyder et al. (1981) for weakly forced waves and Plant (1982) for strongly forced waves, which are thus consistent with available field observations of wave growth.

Additional tests made to assess the robustness of S_{ds}^{B} and the flexibility of its tuning parameters were made using two other input source terms, proposed by Snyder et al. (1981) and Janssen (1991). Both forms are presently used in several versions of operational wind-wave models, such as WAM, WAVEWATCH III and SWAN.

The form of S_{in} from Snyder et al. (1981) (henceforth S_{in}^{S}) is

$$S_{in}^{S}(k,\ \theta) = \frac{\rho_{air}}{\rho_{sea}}0.25\left(\frac{28u_*}{c}\cos\theta - 1\right)\omega F(k,\ \theta). \quad (9)$$

Equation (9) is a parameterization based on the growth rates of moderately forced to mature waves ($1 < U_{10}/c < 3$). This limited range of forcing intensities, which excluded strongly forced waves, led to a parametric form of S_{in} with a linear dependence on the inverse wave-age parameter u_*/c. Although observational evidence gath-

ered more recently supports a quadratic dependence of input rates on inverse wave age at higher wavenumbers, this form of S_{in} is still used in operational wave forecasting applications.

Field experiments reported by Donelan (1982) and Smith et al. (1992) have provided strong evidence that the roughness length z_0 and drag coefficient C_D depend on the sea state, implying that forms of S_{in} specified in terms of friction velocity u_* should also depend on the sea state. The form of S_{in} proposed by Janssen (1991) (henceforth S^J_{in}) incorporates both the concept of a sea-state-dependent u_* and the quadratic dependence of wind input rates on the inverse wave age as follows:

$$S^J_{in} = \frac{\rho_{air}}{\rho_{water}} \beta(\Upsilon, z_0)\Upsilon^2 \omega F(k, \theta), \tag{10}$$

where $\Upsilon = (u_{**}/c + z_\alpha)\cos\theta$, u_{**} is the sea-state-dependent friction velocity, c is the wave phase speed, and $z_\alpha = 0.011$. The growth-rate coefficient (Miles's parameter) in Eq. (10) is $\beta = 1.2/\kappa\mu \ln^4\mu$, where $\kappa = 0.4$ is the von Kármán constant and $\mu = [(gz_0)/c^2]\exp(\kappa/\Upsilon)$, with the roughness length determined from the Charnock relation $z_0 = 0.009u^2_{**}/g$.

Equation (10) is presently used in the WAM Cycle-4 model. The dependence of u_{**} on sea state is calculated through an iterative algorithm that couples the forcing wind field to the high-wavenumber range of the wave spectrum. The implementation in the TR82 model of such a coupled algorithm, as used in WAM Cycle 4, proved sensitive to numerical instabilities at high wavenumbers, leading to unreliable estimates of u_{**} and unrealistic values of spectral energy densities. This was most likely a consequence of either the adopted experimental setup, in which source terms were solved explicitly within a spectral range extending toward very high wavenumbers limited at $25k_p$, and/or the use of an exact solution for the nonlinear interactions term S_{nl}.

A more straightforward approach to calculating u_{**} was thus implemented to overcome the problems of high-wavenumber instabilities. This approach consisted of using the parametric function expressing the sea-state dependence of z_0 proposed by Donelan et al. (1993) as follows:

$$z_0 = 3.7 \times 10^{-5} \frac{U^2_{10}}{g}\left(\frac{U_{10}}{c_p}\right)^{0.9}, \tag{11}$$

with $u_{**} = 0.4U_{10}/\log(10/z_0)$.

Equation (11) is a parametric fit to measurements made during the Humidity Exchange over the Sea (HEXOS) experiment (Smith et al. 1992). According to Janssen (1994), the coupled solution of S^J_{in} used in WAM Cycle 4 gives estimates of u_{**} that are in good agreement with the observed values of this parameter during HEXOS. Therefore, it is reasonable to expect that the input rates computed using Eq. (11) are consistent with those obtained with the coupled solution used in the WAM Cycle-4 model.

Recent advances in understanding the governing mechanisms of the momentum flux from wind to waves have been incorporated in other parameterizations of S_{in}. Major improvements have been the inclusion of the effects of the sea state on spectral rates of wind input (Janssen 1991; Tolman and Chalikov 1996) and the negative air–sea momentum flux for wave components that travel faster than the wind (Tolman and Chalikov 1996; Makin et al. 1995; Donelan 1999). Although evidence on the decay of laboratory waves that propagate faster than or against the wind has been provided recently by Donelan (1999), this negative ''input'' has not yet been observed in the field. Experiments on the effects of including a form of S_{in} that accounts for negative momentum fluxes from spectral components that propagate faster than or against the wind were not investigated here and will be addressed in future research.

b. Discrete wavenumber spectral grid

Although operational wave models limit the explicit computation of source terms to wavenumbers smaller than $6.25k_p$ ($2.5f_p$), the form S^B_{ds} was designed to specify dissipation rates for all scales within the gravity-wave range. Therefore, the appropriate experimental design for assessing its performance included a wavenumber grid in which source terms were computed explicitly up to $k_{max} \gg 6.25k_p$. The extension of this grid toward higher wavenumbers is, however, limited by restrictions on the validity of the Taylor series expansions made in Hasselmann (1962) to obtain the S_{nl} integral. BY94 argue that the limit to the validity of S_{nl} can be expressed in terms of the ratio of the root-mean-square wave height H_{rms} to the shortest wave wavelength λ_{short}, with the cutoff wavenumber at $k_c = 2\pi/\lambda_{short}$. The expansion is valid provided $H_{rms}/\lambda_{short} < O(1)$.

Figure 2 shows the evolution of H_{rms} against inverse wave age U_{10}/c_p of a typical fetch-limited model run and the associated estimates of the ratio k_c/k_p, obtained by using the condition $H_{rms}/\lambda_{short} < O(1)$. Values of k_c/k_p vary from 27 to 63 as the wave field develops from young wind seas toward full development. Based on these results, we set a limiting value for explicitly computing source terms at $k_c = 25k_p$. Thus, the directional wavenumber spectrum $F(k, \theta)$ was represented through a numerical grid consisting of 50 wavenumbers spaced according to $k_n = \xi k_{n-1}$, with the highest wavenumber k_{max} coinciding with the initial value of k_c—that is, $k_{max} = 25k^0_p$ (or $f_{max} = 5f^0_p$)—where k^0_p is the spectral peak wavenumber used to initialize the computations. The lowest wavenumber in the spectral grid was defined as $k_{min} = k_{max}/\xi^{n-1}$, where ξ is a geometric ratio set to 1.166 after extensive sensitivity tests. The wavenumber grid had 53 equal angular bands defined in the range $-120° < \theta < 120°$.

Absolute values of k^0_p were selected to match the nondimensional peak frequency $\nu = f_p U_{10}/g$ corresponding to the lowest nondimensional fetch χ_{min} within the valid range of the Kahma and Calkoen (1992, 1994) evolution

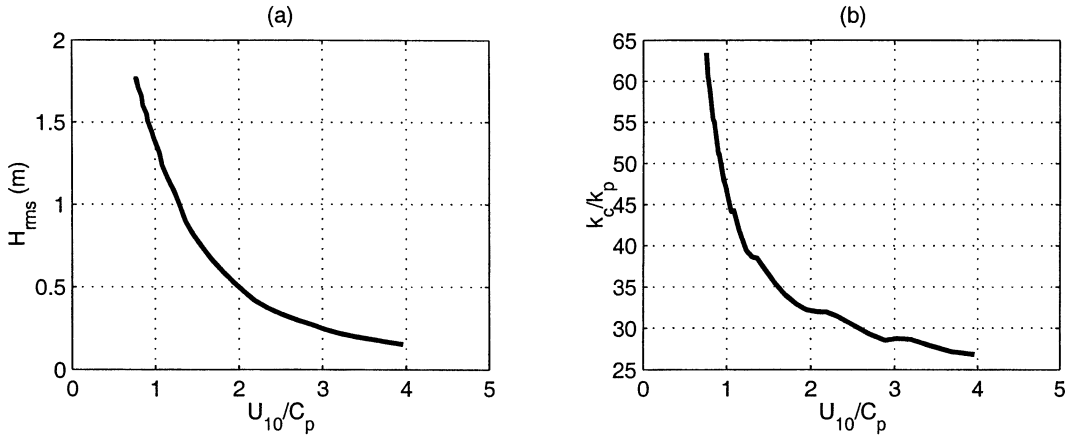

FIG. 2. (a) Root-mean-square wave height H_{rms} vs inverse wave age U_{10}/c_p for typical fetch-limited conditions for $U_{10} = 10$ m s^{-1}. (b) The corresponding ratio k_{max}/k_p computed according to $H_{rms}/\lambda_{short} < O(1)$. The values were obtained from a preliminary numerical experiment using the TR82 code.

curves. Taking U_{10} as the reference wind speed, an initial nondimensional fetch $\chi_{min} = 1 \times 10^2$ resulted in $\nu_{min} = 0.63$, which led to $k_p^0 = g(2\pi\nu_{min}/U_{10})^2$. For $U_{10} = 10$ m s^{-1}, the resulting values for these spectral grid parameters were $f_p^0 = 0.61$ Hz, $k_p^0 = 1.48$ rad m^{-1}, $k_{min} = 0.02$ rad m^{-1}, $k_{max} = 37.09$ rad m^{-1}, $N_k = 50$, and $\xi = 1.166$.

The explicit computations of source terms was made within the bandwidth $0.25k_p < k < k_c$, with $k_c = 25k_p$. Spectral densities were set to 0 below $0.25k_p$ and were prescribed by a diagnostic tail proportional to k^{-4} within $k_c < k < k_{max}$, when applicable. Experiments were initialized at a nondimensional fetch $\chi_{min} = Xg/U_{10}^2 = 1 \times 10^2$, which involved explicit computation of source terms at very high wavenumbers. Because the magnitude of the source terms is generally proportional to a high power of the wavenumber (Phillips 1985), numerical instabilities in the spectral tail were reduced substantially by retaining the time-dependent term $\partial F(k, \theta)/\partial t$ in the numerical solution of Eq. (7), as discussed above.

c. Initial conditions

All model runs were initialized with a Joint North Sea Wave Project (JONSWAP) spectrum (Hasselmann et al. 1973) in which the spectral parameters were specified using slightly modified coefficients in the original expressions derived by Lewis and Allos (1990), thereby providing an optimal match to the Kahma and Calkoen (1992, 1994) fetch-limited evolution curves (see below) at different wind speeds and initial fetches for neutrally stable conditions. Experiments were made with the initial peak frequency $f_p^0 = 0.61$ Hz for $U_{10} = 10$ m s^{-1}.

d. Validation strategy

The model validation strategy consisted of adjusting the parameters of S_{ds}^B until an optimal fit was achieved of model results to observations of fetch-limited wind-wave evolution. We assumed that this optimal fit was reached when the bias was lower than 10% between model outcomes and the observed power-law evolution of the total energy E_{tot} and peak frequency f_p with fetch X, according to parametric curves based on a composite dataset of existing fetch-limited observations proposed by Kahma and Calkoen (1992, 1994, hereinafter KC92/94). In addition, we sought an appropriate transition of these parameters toward the full-development limits of Komen et al. (1984, henceforth KHH) or A00. A secondary goal of our validation strategy was to make a preliminary assessment of the effects of S_{ds}^B on the shape of the wavenumber spectrum.

1) INTEGRAL SPECTRAL PARAMETERS

Our validation approach focused on the computed values of total energy E_{tot} and peak frequency f_p. E_{tot} was determined through discrete integration of the computed wavenumber spectrum $F(k, \theta)$, as follows:

$$E_{tot} = \sum_{k=0.25k_p}^{25k_p} F(k, \theta)k\Delta k\Delta\theta. \tag{12}$$

The peak frequency was derived directly from the dispersion relation $f_p = \sqrt{gk_p}/2\pi$, with peak wavenumber k_p computed according to Young (1995):

$$k_p = \frac{\sum\sum kF^4(k, \theta)\Delta k\Delta\theta}{\sum\sum F^4(k, \theta)\Delta k\Delta\theta}. \tag{13}$$

Model predictions of fetch-limited spectral integral parameters were compared with the following expressions fitting the composite dataset of fetch-limited wave observations of KC92/94, according to the scaling wind speed U_0 used in the definition of S_{in}, as follows:

1) $U_0 = u_*$,

$$\varepsilon_* = E_{\text{tot}} g^2/u_*^4 = \min(6.5 \times 10^{-4}\chi_*^{0.9}, \varepsilon_*^{\text{FD}}), \quad (14)$$

and

$$\nu_* = f_p u_*/g = \max(4.90 \times 10^{-1}\chi_*^{-0.27}, \nu_*^{\text{FD}}), \quad (15)$$

where $\chi_* = Xg/u_*^2$ and u_* is a sea-state-independent friction velocity used in the wind input functions S_{in}^S and S_{in}^Y. These parametric curves were used to assess model results within the active fetch-limited growth range (i.e., $1 \times 10^5 \le \chi_* \le 3 \times 10^6$). Near full development, model outcomes were compared with two alternative sets of asymptotic levels provided by KHH ($\varepsilon_*^{\text{FD}} = 1.10 \times 10^3$ and $\nu = 5.60 \times 10^{-3}$) and A00 ($\varepsilon_*^{\text{FD}} = 1.62 \times 10^3$ and $\nu_*^{\text{FD}} = 5.31 \times 10^{-3}$).

2) $U_0 = u_{**}$,

$$\varepsilon_{**} = E_{\text{tot}} g^2/u_{**}^4 = \min(6.5 \times 10^{-4}\chi_{**}^{0.9}, \varepsilon_*^{\text{FD}}), \quad (16)$$

and

$$\nu_{**} = f_p u_{**}/g = \max(4.90 \times 10^{-1}\chi_{**}^{-0.27}, \nu_*^{\text{FD}}), \quad (17)$$

where u_{**} is a sea-state-dependent friction velocity calculated using Eq. (11). Again, these curves were used to assess model results within the active fetch-limited growth range, $1 \times 10^5 \le \chi_* \le 3 \times 10^6$. The asymptotic full-development levels $\varepsilon_*^{\text{FD}}$ and ν_*^{FD} from KHH and A00 were the same as those used in association with Eqs. (14) and (15). This set of benchmark curves was used to assess model runs made with S_{in}^J.

2) Assessment of spectral shape

The shape of model spectra was assessed in terms of a parameterization of the high-wavenumber equilibrium range based on the directional wavenumber spectral model of Banner (1990, henceforth B90). This parameteric equilibrium-range model is defined in terms of the average spectral tail level $\overline{\alpha}_B$ and the average spectral tail slope exponent $\overline{n}_B$ of the slice of the directional wavenumber spectrum in the wind direction. A third validation parameter based on B90 was the relative energy density ratio ϵ_B between the model wavenumber spectral slice in the wind direction and its empirical counterpart according to B90.

Empirical values for parameters used to assess the shape of the high-frequency tail in model spectra are derived from the following power-law representation:

$$F_B(k, \theta_{\text{wind}}) = \overline{\alpha}_B u_*^{-2(\overline{n}_B+4)} g^{(\overline{n}_B+4)} k^{\overline{n}_B}, \quad (18)$$

where θ_{wind} is the direction of wave components aligned with the wind direction. B90 found that observed values for the average spectral tail slope exponent and the average spectral tail level were $\overline{n}_B = -4$ and $\overline{\alpha}_B = 4.5 \times 10^{-5}(U_{10}/c_p)^{1/2}$, respectively.

The parameter ϵ_B, which measures the magnitude of computed spectral tail energy levels relative to the parametric equilibrium range model of B90, is given by

$$\epsilon_B = \frac{F(k, \theta_{\text{wind}})}{F_B(k, \theta_{\text{wind}})}. \quad (19)$$

Values of $\overline{\alpha}_B$ and $\overline{n}_B$ were calculated from model spectra using a least squares fit to wavenumbers within $6.25\, k_p \le k \le 25 k_p$. Relative energy levels ϵ_B were calculated at $4k_p$ and $9k_p$.

3) Directional spread

A straightforward measure for validation of directional properties of model spectra is the mean spectral width $\overline{\theta}$, given by

$$\overline{\theta}(k) = \frac{\int_0^\pi \theta F(k, \theta)\, d\theta}{\int_0^\pi F(k, \theta)\, d\theta} = \frac{\int_0^\pi \theta D(k, \theta)\, d\theta}{\int_0^\pi D(k, \theta)\, d\theta}. \quad (20)$$

Empirical values of $\overline{\theta}$ were obtained by integrating two alternative parameterizations of $D(k, \theta)$ from Donelan et al. (1985) and Babanin and Soloviev (1998) using Eq. (20).

4) High-resolution directional data

Hwang et al. (2000a,b) recently published results of high-resolution measurements of open-ocean wind-wave topography, made with an airborne scanning laser device known as airborne topographic mapper (ATM). This novel technique provides directional wavenumber spectra with significantly higher directional resolution than previously available techniques, allowing direct validation of model predictions of the directional properties of wave spectra. The reader is referred to their papers for details on the measurement technique.

A striking aspect of wave spectra obtained from ATM measurements is a strong bimodal directional signature above $k/k_p \approx 3$. This was noted as a persistent feature in the computations of BY94, but had not been unequivocally confirmed in field data from sparse wave gauge arrays, potentially masked by their limited angular resolution. In any event, we provide a preliminary intercomparison of model results with this initial set of ATM measurements but look to a future larger ensemble of ATM measurements for a more definitive study.

The comparisons made below are based on two key angular spreading properties reported in Hwang et al. (2000b): the dependences on k/k_p of 1) the spreading angle of the local maximum spectral level θ_{lobe} and 2)

the lobe ratio $r_{\text{lobe}} = F(k, \theta_{\text{lobe}})/F(k, \theta_{\text{wind}})$, which reflects the peakedness of the maximum spreading relative to the mean direction. Validation of model outputs is made considering spectra with a wave age consistent with the quasi-steady conditions observed by Hwang et al. (2000a) (i.e., $c_p/U_{10} \approx 1.02$).

e. Name convention for model runs

Model runs were named according to the following convention: the first character identifies the form of S_{ds} (B for the saturation-based form S_{ds}^{B} or W for the WAM Cycle-4 form S_{ds}^{W4}); the following character identifies the wind input form, being either Y, S, or J for S_{in}^{Y}, S_{in}^{S}, or S_{in}^{J}, respectively; the remaining characters identify particular properties of each individual test, such as particular parameter values or a property of the target benchmarks used for model validation, for example.

5. Summary and updates to BY94

Our approach to assess the performance of the saturation-based dissipation source term S_{ds}^{B} follows the investigation of BY94, who provide an extensive performance analysis of S_{ds}^{W3}. Since BY94 was published, a more recent version of the WAM model, Cycle 4, was released (Günther et al. 1992) and has progressively replaced the previous WAM model version in operational applications. WAM Cycle 4 is a technically enhanced version of Cycle 3 that includes the wind input source term S_{in}^{J} and the form S_{ds}^{W} with $\delta = 0.5$ [see Eq. (2)]. Thus, for the purposes of providing an updated reference framework to assess the performance of S_{ds}^{B}, we present a brief overview of the impact of using the WAM Cycle-4 parameterization of S_{ds}^{W} to model performance relative to the results of BY94, which are also briefly reviewed.

a. Major findings of BY94

Using the two wind input source terms S_{in}^{S} and S_{in}^{Y} and the TR82 model with its exact nonlinear S_{nl} algorithm, BY94 investigated the performance of a wide range of configurations for the quasi-linear form S_{ds}^{W3} in simulations of fetch-limited wind-wave growth by changing the values of C_{ds} and n in Eq. (2). Despite an extensive effort, their model results failed to reproduce the observed evolution curves for fetch-limited integral spectral parameters of Kahma and Calkoen (1992).

When dissipation rates were set to provide model results that match the empirical growth curves at short fetches, the growth rates would become too low at long fetches, with significant underprediction of asymptotic wave energy levels near full development. Conversely, when dissipation rates were reduced to allow a proper transition toward full development, growth rates became too large at short fetches, resulting in an overprediction of wave energy for young wind seas. This behavior is analogous to that of the default configuration of S_{ds}^{W4} used presently in the WAM model (see below), which is illustrated in Fig. 3.

BY94 showed that S_{ds}^{W3} failed to reproduce properties related to the shape of fetch-limited spectra, because model spectra did not reproduce the spectral tail levels $\overline{\alpha}_B$ and the slope exponent $\overline{n}_B = -4$ prescribed by the parametric equilibrium range model of B90. BY94 also reported values of ϵ_B typically around 2—that is, tail energy levels in model spectra that were 2 times as large as the observed values according to B90. Further, the directional width of model spectra was broader at the spectral peak wavenumber k_p and narrower at high wavenumbers relative to observational data. These findings are consistent with the analysis of the performance of S_{ds}^{W4} presented below, as illustrated in Figs. 6 and 7.

b. WAM Cycle-4 dissipation rates

The dissipation-rate source term used in the WAM Cycle-4 model is a variation of S_{ds}^{W} (hereinafter represented by the symbol S_{ds}^{W4}) designed to compensate for the higher S_{in}^{J} rates within the spectral tail relative to the form S_{in}^{S} used in previous versions of WAM. Here S_{ds}^{W4} prescribes dissipation rates that are similar to S_{ds}^{W3} at the spectral peak, but larger dissipation rates are obtained toward the spectral tail as a consequence of using $\delta = 0.5$ in the linear combination $(1 - \delta)k/\overline{k} + \delta(k/\overline{k})^2$. The resulting form S_{ds}^{W4} is, therefore, still consistent with the hypothesis of Hasselmann (1974) of quasi-linear dissipation rates across the wave spectrum.

A00 showed that S_{in}^{J} predicts growth rates that are generally consistent with those provided by the form S_{in}^{Y} of Yan (1987). The main reason for the similarities is that in both cases the quadratic dependence of S_{in} on the inverse wave age u_*/c_p results in higher input rates at the spectral tail relative to the form S_{in}^{S} used in WAM Cycle 3. Taking this qualitatively similar behavior of S_{in}^{J} and S_{in}^{Y} into account, we use the numerical modeling approach outlined in section 3 to provide a performance assessment of the WAM Cycle-4 model physics that updates the results of BY94, focusing on the advances incorporated into S_{ds}^{W4}.

1) Integral spectral parameters

Comparisons of integral spectral parameters from a model run made with the default configuration of S_{ds}^{W4}, for example, $C_{\text{ds}} = 9.4 \times 10^{-5}$, $m = 2$ and $\delta = 0.5$, are shown in Fig. 3. Following our run-code convention, this run was labeled WYM2. Predicted values of ε_* and ν_* associated with WYM2 diverged from the power-law behavior of the target evolution curves within the valid range of fetch-limited observations. The percentage bias for ε_* indicated an underprediction of up to 40% while calculated ν_* values overpredicted the observations by up to 8%. Results of run WYM2 provided a full-development limit close to $\varepsilon_*^{\text{FD}} = 7 \times 10^{-2}$, which

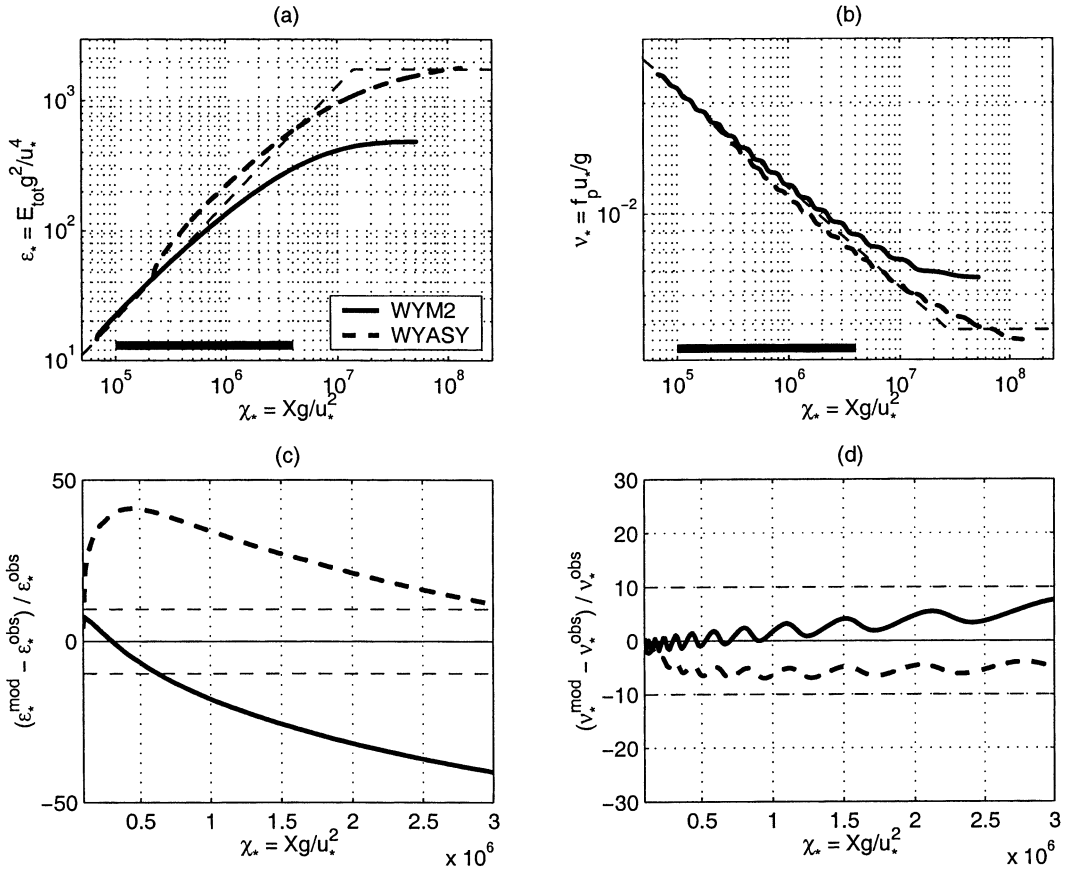

FIG. 3. Model runs made with S_{ds}^{W4} and S_{in}^{Y}: WYM2 (continuous lines) and WYASY (broken lines). The upper diagrams show the evolution of (a) nondimensional total energy ε_* and (b) nondimensional peak frequency ν_*. Comparisons are made with the evolution curves of KC92/94 and the asymptotic limit of A00 (thin dashed lines). (c), (d) The percentage bias of model results to the KC92/94 curves within the valid range of fetch-limited observations (thick horizontal lines indicated in the upper panels).

is significantly lower than the asymptotic limits proposed by KHH and A00. The asymptotic value for $\nu_* = 6.9 \times 10^{-3}$ was also significantly higher than the empirical asymptotes of KHH and A00.

A variation of run WYM2 consisted of reducing C_{ds} without changing other parameters to allow the growth of model E_{tot} closer to the chosen empirical full-development limits. Parameter values of S_{ds}^{W4} were set to $C_{ds} = 1.80 \times 10^{-5}$, $m = 2$ and $\delta = 0.5$, and the experiment was labeled WYASY. Consistent with the results of BY94, WYASY predicted dissipation rates that become too low at shorter fetches, with overprediction of ε_* reaching 50%. Conversely, predicted ν_* underestimated observed values by approximately 5% at short fetches and 10% at full development.

To investigate the effect of increasing the nonlinear dependence of S_{ds}^{W4} on $(E_{tot}\overline{k}^2/\alpha_{PM})^m$, experiments WYM3, WYM4, and WYM5 were made with the exponent m set to 3, 4, and 5, respectively. Values of the dissipation constant C_{ds} were also changed to accommodate the new exponents. These new values for C_{ds} were 2.4×10^{-5}, 1.20×10^{-5}, and 8.00×10^{-6}, respectively. The results, shown in Fig. 4, indicate that increasing the values of m generally reduced the bias of computed ε_* and ν_* relative to the empirical evolution curves. The percentage bias, however, was still high for $m \leq 3$. With $m = 4$, the maximum percentage bias of ε_* and ν_* were reduced to less than 15% and 3%, respectively. Furthermore, the computed asymptotic limits of these two integral parameters approached very closely the full-development asymptotes of KHH. When an exponent $m = 5$ was used, however, the growth of ε_* overshot both this limit and the asymptote of A00.

The results described so far indicate that tuning the exponent m in S_{ds}^{W4} provides a potential way of optimizing model performance in terms of spectral integral quantities. Depending on the choice of m, however, the percentage bias of computed spectral integrals at shorter fetches may become too large. In addition, high values of m in S_{ds}^{W4} led to the continuous growth of E_{tot} beyond the full-development limits because of an imbalance between S_{ds} and S_{nl} around the spectral peak, at very long fetches. These limitations indicate that changes in m alone do not provide enough flexibility to adjust S_{ds}^{W4}.

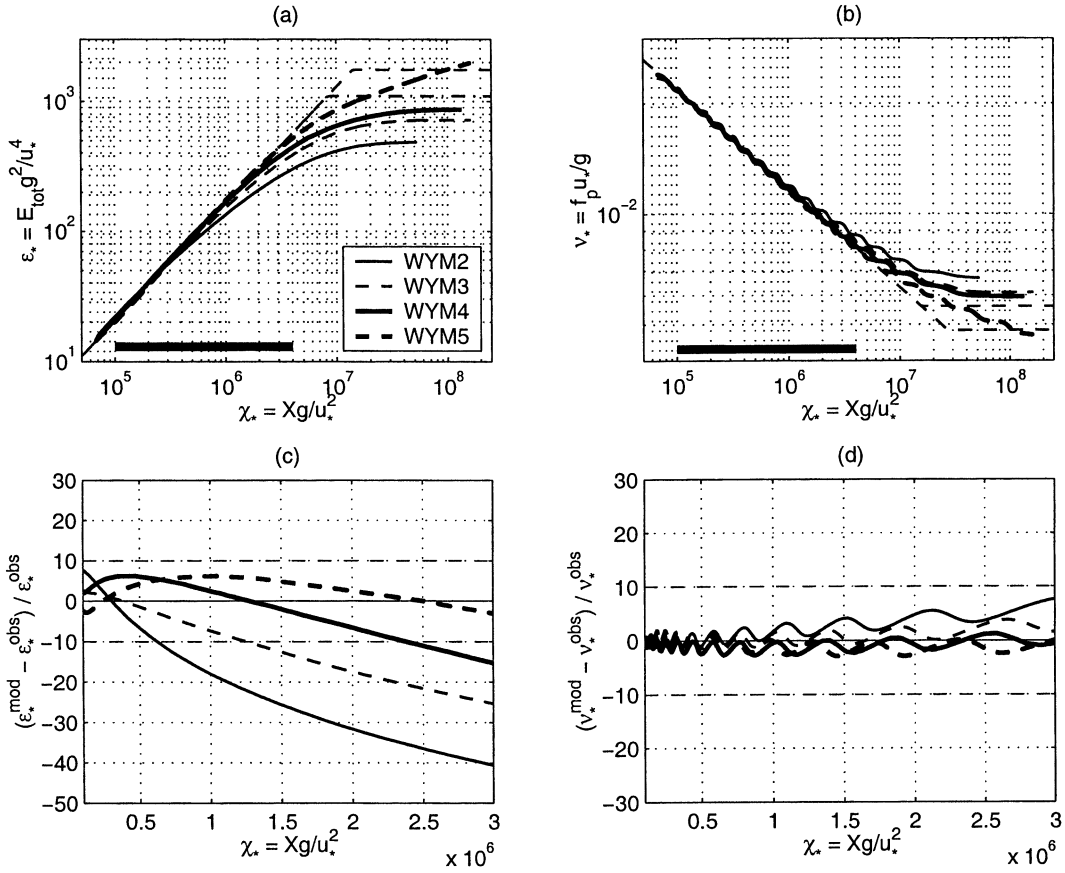

FIG. 4. Model runs made with S_{ds}^{W4} and several values of m. The upper diagrams show the evolution of (a) nondimensional total energy ε_* and (b) nondimensional peak frequency ν_*. The empirical KC92/94 curves are shown as dashed lines, along with the full-development asymptotes of KHH (lower broken line) and A00 (upper broken line). (c), (d) The percentage bias of model results relative to the KC92/94 curves within the valid range of fetch-limited observations (thick horizontal lines indicated in the upper panels).

Further modifications in S_{ds}^{W4} were made by setting δ to values ranging from 0.3 to 0.6. These additional model runs were made with $m = 4$, because this choice of exponent provided a reasonably good fit of model results to the empirical curves of KC92/94 and to the asymptotic limit of KHH. Runs with several values of δ are indicated by the two-character suffixes D3, D4, and D6 added to WYM4, corresponding to values of $\delta = 0.3$, 0.4 and 0.6, respectively, whereas the code WYM4 without a suffix indicates the run made with $\delta = 0.5$.

Results shown in Fig. 5 indicate that the changes in δ had only a marginal effect in the computations of ε_* and ν_* within the valid range of the target fetch-limited curves. The percentage bias of ε_*, however, was slightly reduced when δ was set to 0.3 (run WYM4D3). These outcomes of run WYM4D3 were also closer to the full-development limit of ε_* proposed by KHH. These results confirm the study by Hersbach (1998), who determined an optimal value of $\delta = 0.31$ on the basis of inverse wave modeling, using an adjoint version of the WAM model. These results for spectral integral quantities calculated with S_{ds}^{W4} indicate a significant improvement relative to the predictions of spectral integrals obtained with S_{ds}^{W3} reported in BY94.

2) SPECTRAL TAIL PARAMETERS

Figure 6 shows predictions of diagnostic spectral tail parameters calculated using S_{ds}^{W4}. This figure includes results from runs WYM4, WYM4D3, WYM4D4, and WYM4D6. A general feature of Fig. 6 is that the model results from all these cases were significantly different from the values of the B90 empirical spectral tail diagnostic parameters indicated in the figure, repeating the poor performance of S_{ds}^{W3} reported in BY94.

Run WYM4, made with the default configuration of S_{ds}^{W4}, produced a spectral tail that was too steep in early development stages ($\overline{n}_B \approx -4.4$ at $c_p/u_* \approx 10$) and too gentle at full development ($\overline{n}_B \approx -3.75$ at $c_p/u_* \approx 25$); B90 proposes a constant slope $\overline{n}_B = -4$. Values of $\overline{\alpha}_B$ were consequently 1.4–2 times as large as predicted by B90. Values of ϵ_B from WYM4 at $k = 4k_p$ ranged from 1.5 to 1.8 times the empirical value of B90. This departure from the expected behavior according to B90

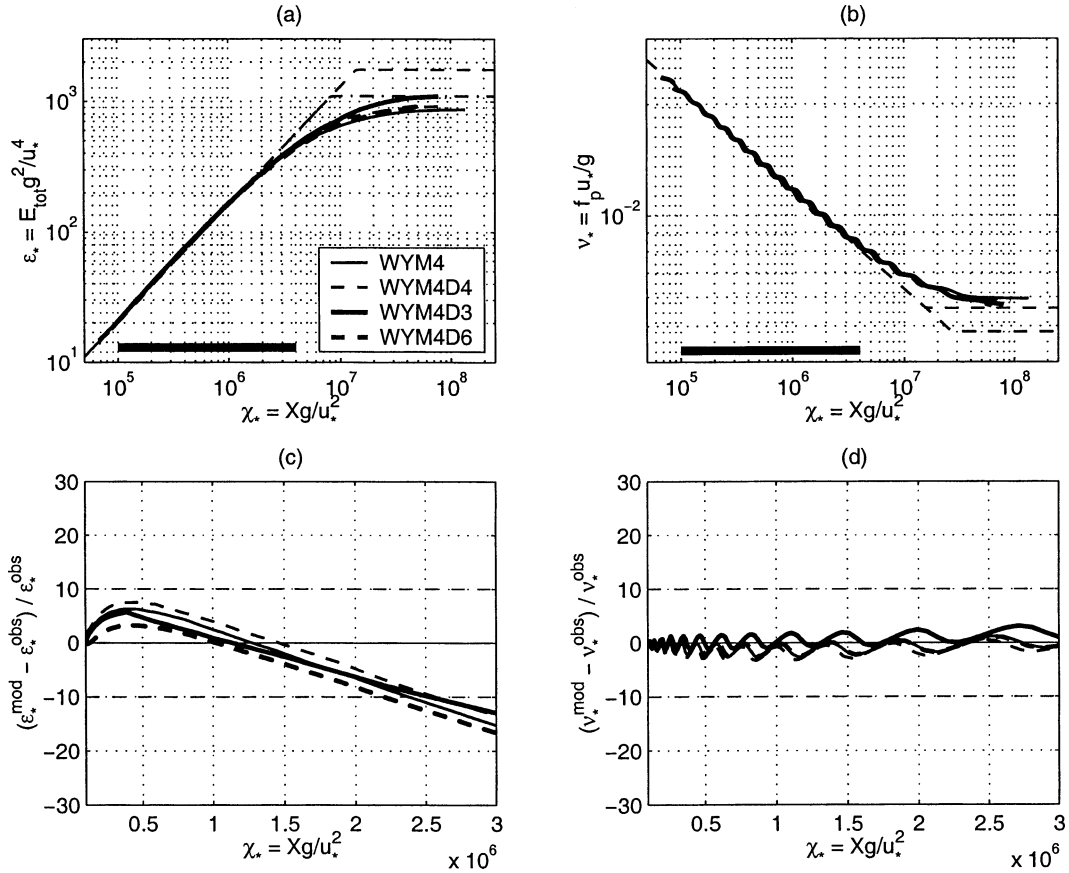

FIG. 5. Model runs made with S_{ds}^{W4} and several values of the weighting factor δ. The upper diagrams show the evolution of (a) nondimensional total energy ε_* and (b) nondimensional peak frequency ν_*. The empirical KC92/94 curves are shown as dashed lines, along with the full-development asymptotes of KHH (lower broken line) and A00 (upper broken line). (c), (d) The percentage bias of model results relative to the KC92/94 curves within the valid range of fetch-limited observations (thick horizontal lines indicated in the upper panels).

was even stronger at $k = 9k_p$, where ϵ_B ranged from 0.9 to 2 times the empirical values. Similar results were obtained with other model runs using $\delta = 0.5$ and different values of m.

Smaller discrepancies between model results and empirical spectral tail parameters were obtained using $\delta = 0.3$ in run WYM4D3, as seen in Fig. 6. This more stable behavior, however, resulted in an average tail slope ($\overline{n}_B \approx -3.7$) that was less steep than the empirical value $\overline{n}_B = -4$. Associated values of $\overline{\alpha}_B$ agreed well with B90. Nevertheless, model predictions of ϵ_B were 2 times as large as the empirical value of B90 at $4k_p$ and 2.5 times as large at $9k_p$.

Increasing the value of δ to 0.6 (run WYM4D6) resulted in a much stronger disagreement of model results with the empirical relations proposed by B90. Although values of $\overline{n}_B$ were close to -4 near full development, they were as low as -5 in earlier development stages. Values of $\overline{\alpha}_B$ were significantly higher than observations, and energy densities in the wind direction slice at $4k_p$ and at $9k_p$ also diverged from the empirical values of B90. We conclude that S_{ds}^{W4} brings no significant improvement to model performance in terms of predictions of spectral shape relative to the results from BY94 on using S_{ds}^{W3}.

3) DIRECTIONAL SPREAD

Computed mean directional spreading of spectra generated by experiments made with S_{ds}^{W4} are shown in Fig. 7. This figure indicates that the agreement of $\overline{\theta}$ from most model runs made with various configurations of S_{ds}^{W4} was generally poor. Figures 7a,b show the results of runs WYM2, WYM4, and WYM5. These diagrams indicate that higher values of m provided computed θ that were closer to the areas representing empirical data at the spectral peak, particularly in the case of run WM5. On the other hand, increasing the values of m led to a stronger overall disagreement with observations of $\overline{\theta}$ at $4k_p$.

Figures 7c,d show the results of runs WYM4, WYM4D3, and WYM4D6, revealing that the variation

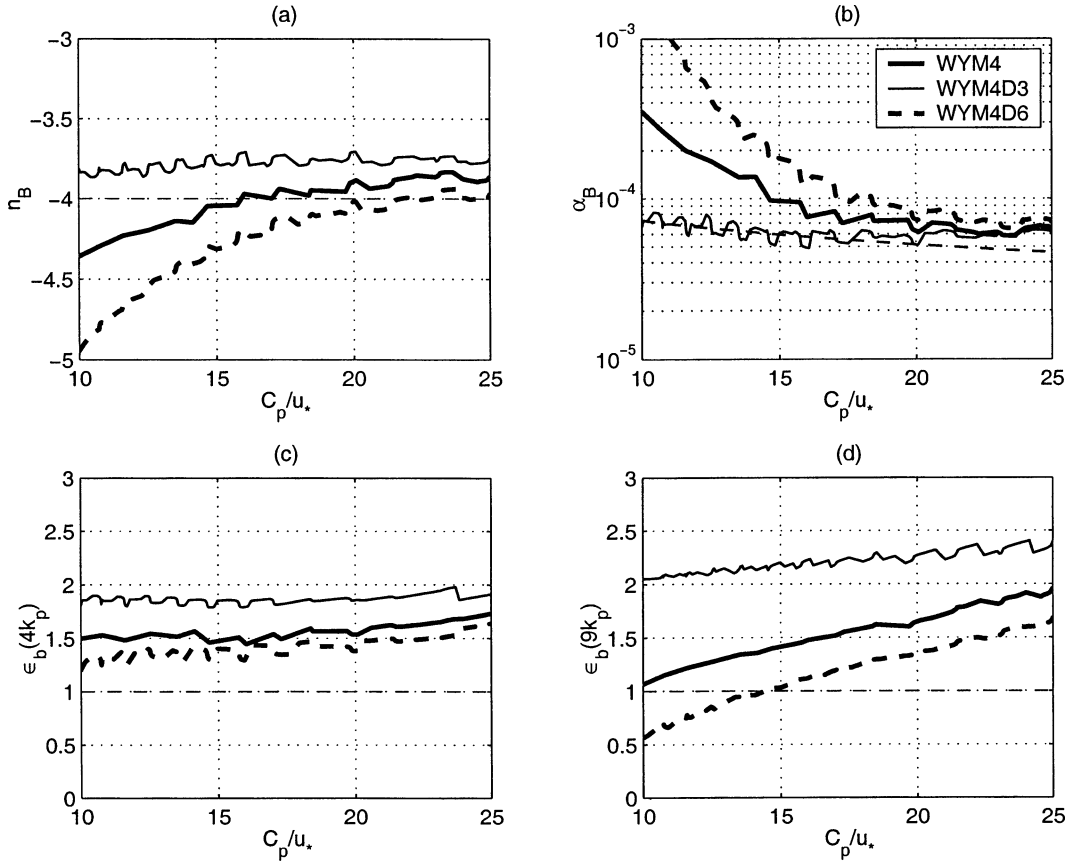

FIG. 6. Spectral tail evolution from runs made with S_{ds}^{W4} and several values of δ vs the empirical parameters of Banner (1990) (thin broken lines): (a) average spectral tail level $\overline{\alpha}_B$ and (b) average spectral tail slope $\overline{n}_B$ and relative energy density ratio ϵ_B of the wavenumber spectral slice in the wind direction at (c) $k = 4k_p$ and (d) $k = 9k_p$.

of δ had very little effect on the values of $\overline{\theta}$ at the spectral peak relative to other model runs. This result was expected, because at the spectral peak $(1 - \delta)k/\overline{k} + \delta(k/\overline{k})^2 \approx 1$ regardless of the value of δ. The mean directional spreading at $4k_p$, however, was relatively improved when the linear combination weighting parameter was reduced from $\delta = 0.5$ to $\delta = 0.3$. Nevertheless, these results indicate that in terms of directional spectral properties S_{ds}^{W4} does not improve the performance of S_{ds}^{W3} as reported in BY94.

4) HIGH-RESOLUTION DIRECTIONAL DATA

Figure 8a shows the results of a comparison between the spreading angles of local spectral maxima θ_{lobe} and lobe ratios r_{lobe} calculated with S_{ds}^{W4} and the high-resolution directional data of Hwang et al. (2000b), measured for a mature wind sea with quasi-steady $U_{10} \approx 9.5$ m s^{-1}. Model runs using S_{ds}^{W4} provided θ_{lobe} that were in very good agreement with observations both at the transition from a unimodal behavior in the spectral peak toward bimodality and at higher wavenumbers. On the other hand, the agreement of calculated r_{lobe} with the observations of Hwang et al. (2000b), shown in Fig. 8b, is less compelling. In general, model predictions of r_{lobe} were significantly lower than the measured values.

6. Performance of a saturation-based S_{ds}

The performance of the saturation-based dissipation source term S_{ds}^{B} was assessed in terms of numerical simulations of fetch-limited wind-wave evolution made with the TR82 model, following the validation strategy outlined in section 4. Initial experiments were made with wind input rates prescribed by S_{in}^{Y}. Further tests investigated the effects of using S_{ds}^{B} in conjunction with S_{in}^{S} and S_{in}^{J}. Our main objective was to assess S_{ds}^{B} in terms of its ability to provide model results in agreement with the KC92/94 growth curves and with the two alternative full-development asymptotes of KHH and A00. The results described in this section are based on experiments made with a single forcing wind speed, $U_{10} = 10$ m s^{-1}. Although further experiments were made with $U_{10} = 7.5$ and $U_{10} = 15$ m s^{-1}, these are not included here because their results were consistent with runs made

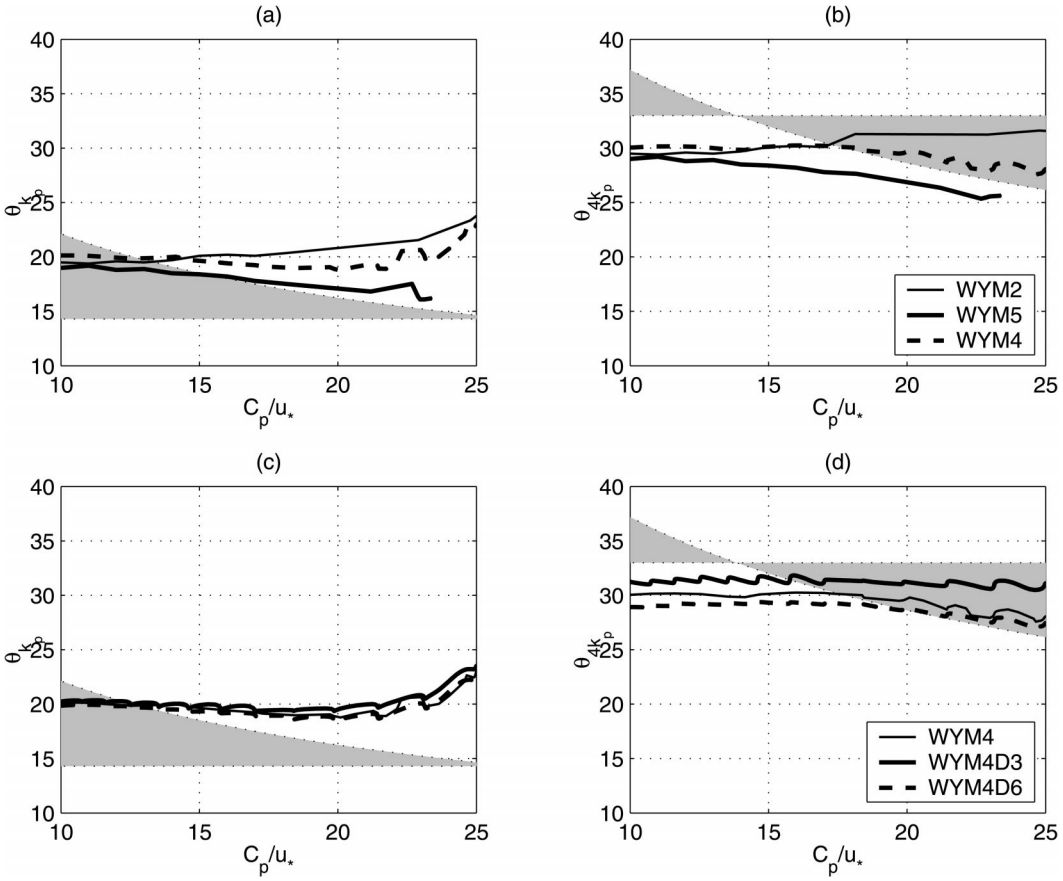

FIG. 7. Mean directional spreading width $\overline{\theta}(k)$ for runs made with S_{ds}^{W4}. Validation is made against a combination of empirical mean spreading widths, resulting in the range indicated by the hatched gray area. Computed $\overline{\theta}(k)$ at k_p and at $4k_p$ are shown in the left- and right-hand panels, respectively.

with $U_{10} = 10$ m s^{-1} in terms of nondimensional spectral integral quantities.

We also provide a preliminary assessment of model results in terms of spectral shape. Following BY94, the assessment of spectral shapes in the high-frequency spectral tail focused only on experiments made with S_{in}^{Y}. A more detailed investigation of the effects to spectral shape and directional spread of using alternative forms of the wind input source function is currently being undertaken. We conclude this section by pre-

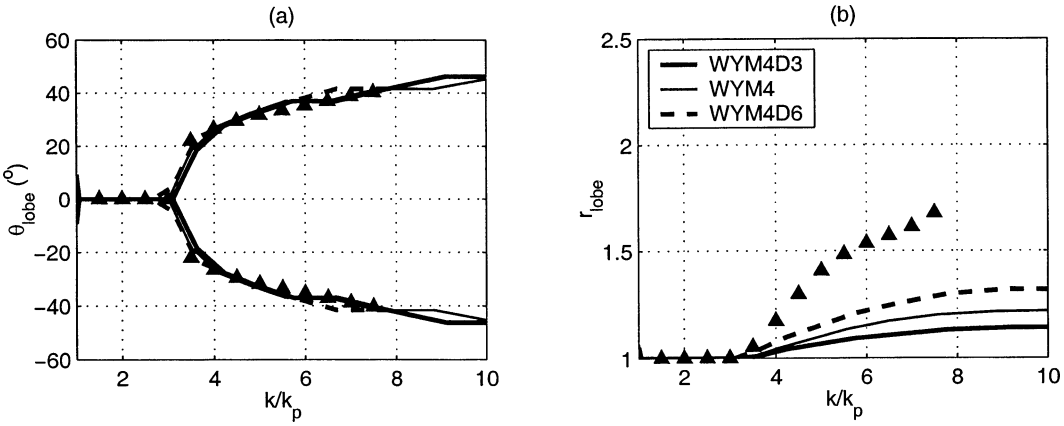

FIG. 8. Calculated (left) θ_{lobe} and (right) lobe ratios r_{lobe} from runs made with S_{ds}^{W4} vs data from Hwang et al. (2000b). Measurements are indicated with triangles.

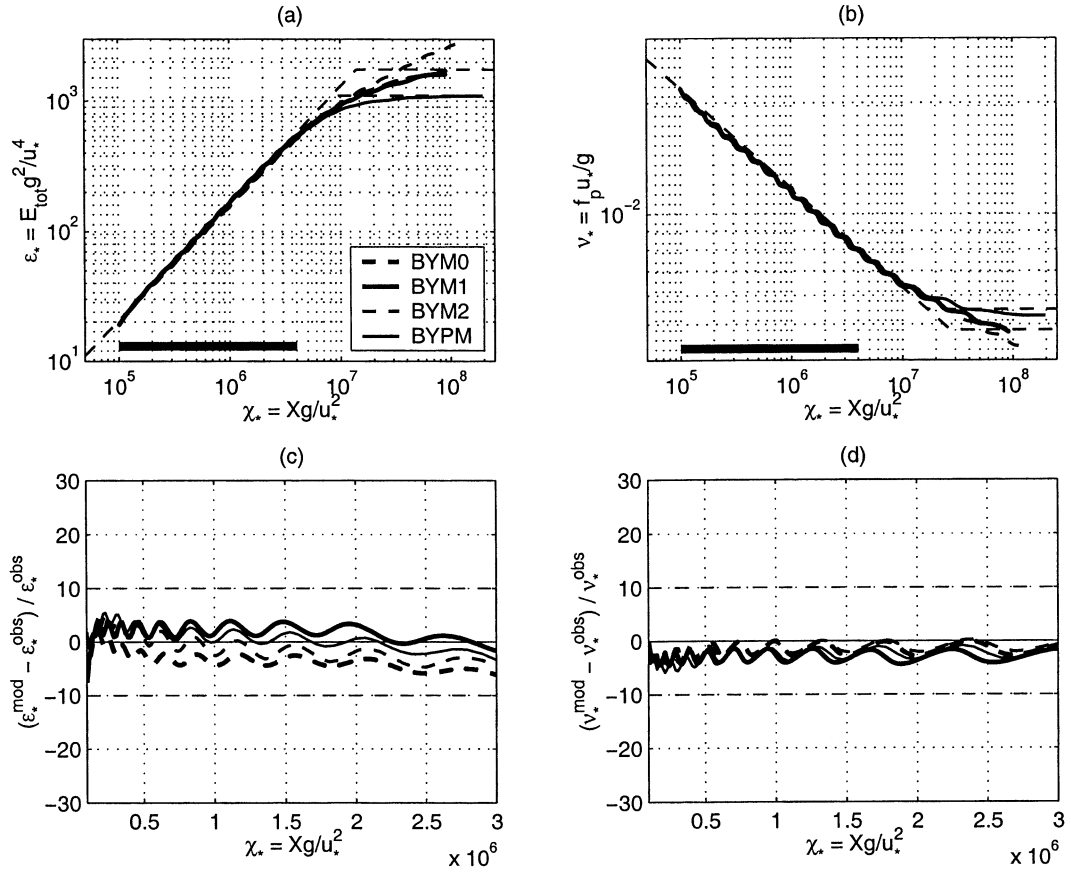

FIG. 9. Model runs BYM1, BYM0, BYM2, and BYPM made with S_{ds}^B. Upper diagrams show the evolution of (a) nondimensional total energy ϵ_* and (b) nondimensional peak frequency ν_*. The empirical KC92/94 curves are shown as dashed lines along with the full-development asymptote of A00. (c), (d) The percentage bias of model results relative to the KC92/94 curves within the valid range of fetch-limited observations (thick horizontal lines indicated in the upper panels).

senting a short description of results on how model spectra produced with S_{ds}^B and the forms of S_{in} discussed above compare with empirical data representing observations of directional energy spread.

a. Spectral integral quantities

1) EXPERIMENTS WITH S_{in}^Y

A first model run made with S_{ds}^B and input rates specified through S_{in}^Y was labeled BYM0. After some adjustments and sensitivity tests, run BYM0 had the following parameter values for S_{ds}^B: $C_{ds} = 1.25 \times 10^{-5}$, $p_0 = 8$, $m = 0$, $n = 2$, and $B_r = 3.38 \times 10^{-3}$. Taking $m = 0$ assumes that background dissipation rates do not depend on the integrated steepness parameter $E_{tot}k_p^2$. As a consequence, the overall spectral dissipation rates prescribed by S_{ds}^B become strongly dependent on the relative saturation parameter $[B(k)/B_r]^{p/2}$.

Results of run BYM0, shown in Fig. 9, indicate that this initial configuration of S_{ds}^B led to a percentage bias within $\pm 10\%$ between model and empirical evolution curves for ϵ_* and ν_*, indicating very good agreement for the fetch-limited growth range. At full development, model results from this run were also in good agreement with the full-development limits reported in A00. These results are very encouraging, because they show that a dependence of dissipation rates solely on the saturation parameter provides good predictions of observed spectral integral quantities.

Before continuing with our presentation of model results, we note that small oscillations in the simulated evolution curves of ϵ_* and ν_* are seen in the results of experiments made with S_{ds}^B. These oscillations appear as a consequence of the nonlinearity of S_{ds}^B and of numerical adjustments of dissipation rates to the abrupt shifting of k_p as its numerical value ''jumps'' from one discrete spectral grid node to the next. The use of a higher-resolution spectral grid in the TR82 model may reduce these oscillations. However, this was not pursued because the associated increase in computational time cost was not compensated by significant changes to model results.

The effect of including a linear dependence of S_{ds}^B on $E_{tot}k_p^2$ was investigated in run BYM1. The following

values of S_{ds}^{B} parameters were found to provide an optimal match of model results to the validation curves: $C_{ds} = 9.25 \times 10^{-3}$, $p_0 = 6$, $m = 1$, $n = 2$, and $B_r = 4.25 \times 10^{-3}$. Results shown in Fig. 9 indicate a slightly improved agreement with observations of ϵ_* and ν_* relative to run BYM0. Predictions of the full-development limits were also in good agreement with the empirical values of A00.

Runs BYM0 and BYM1 indicated that including a dependence of S_{ds}^{B} on the steepness parameter $E_{tot}k_p^2$ provided a means of optimizing model results. Sensitivity tests indicated that this stronger dependence of S_{ds}^{B} on $E_{tot}k_p^2$ led to augmented dissipation rates at shorter fetches and, at the same time, reduced rates near full development. This dynamic behavior of $E_{tot}k_p^2$ is similar to that of the integral steepness parameter $E_{tot}\overline{k}^2$ used in S_{ds}^{W}, as seen in section 5.

The effect of further increasing the dependence of S_{ds}^{B} on $E_{tot}k_p^2$ was investigated in run BYM2. This run had $m = 2$, which required changing other dissipation parameters of S_{ds}^{B} as follows: $C_{ds} = 2.87$, $p_0 = 4$, and $B_r = 3.38 \times 10^{-3}$. The exponent $n = 2$ was left unchanged. Results shown in Fig. 9 indicate that the computed integral spectral parameters were still in good agreement with the target evolution curves at early and intermediate stages of development. However, as the wave field evolved toward full development, the wave spectrum continued to grow beyond the full-development limits. This behavior, analogous to that seen in run WYM5 made with S_{ds}^{W4}, is a consequence of the higher nonlinear dependence of S_{ds}^{B} on $E_{tot}k_p^2$, which results in a sharp reduction of overall dissipation rates near full development, leading to an unbounded net positive flux of energy provided by the positive lobe of S_{nl} toward the spectral peak.

A final experiment with wind forcing specified by S_{in}^{Y} consisted of readjusting S_{ds}^{B} to seek a fit of model results to the full-development limit of KHH, which is approximately 30% lower than the asymptotic level reported in A00. Dissipation parameters were set to $C_{ds} = 3.25 \times 10^{-3}$, $p_0 = 8$, $B_r = 4.12 \times 10^{-3}$, and $m = 0.35$. Results of this model run, labeled BYPM, also shown in Fig. 9, indicate that the readjustments made in S_{ds}^{B} provided the proper dissipation rate levels for producing model outcomes in agreement with the full-development asymptotes of KHH for both ϵ_* and ν_* while still reproducing closely the empirical fetch-limited curves of KC92/94 at all other stages of evolution.

2) EXPERIMENTS WITH S_{in}^{S}

An initial model run using S_{ds}^{B} with wind input rates specified by S_{in}^{S} was labeled BS. In this run, parameters of S_{ds}^{B} were adjusted to provide model results that reproduced closely the evolution of spectral integrals toward the full-development asymptotes of KHH. Because of the weaker input rates of S_{in}^{S} at wavenumbers higher than the spectral peak, dissipation rates in the high-frequency spectral tail were reduced relative to other runs made with S_{ds}^{B} and S_{in}^{Y} or S_{in}^{J}. This was achieved by setting the exponents n and p_0 to 1 and 4, respectively. After some tuning, other parameters of S_{ds}^{B} were set to $C_{ds} = 3.70 \times 10^{-4}$, $m = 0.3$, and $B_r = 3.80 \times 10^{-3}$.

A comparison of computed ϵ_* and ν_* from run BS against the target empirical evolution curves of KC92/94 and the full-development limit of KHH is shown in Fig. 10. Model results are in good agreement with observations within the valid range of these empirical curves, as indicated by a relative bias below 10% for ϵ_* and 5% for ν_*, within the valid range of the KC92/94 evolution curves. Near full development, model results make a smooth transition toward the desired asymptotic levels prescribed by KHH.

A secondary run, labeled BSA, was made to verify the flexibility of S_{ds}^{B} by adjusting its parameters to match the KC92/94 curves, still using S_{in}^{S}, but now targeting the full-development asymptotes of A00. Parameters of S_{ds}^{B} were adjusted until the following configuration was found to provide the best outcomes: $C_{ds} = 4.00 \times 10^{-3}$, $m = 0.8$, and $B_r = 3.80 \times 10^{-3}$. Results, also shown in Fig. 10, again demonstrate good agreement between model calculations of spectral integrals and the target validation curves throughout the active fetch-limited growth range and up to the full-development asymptotes of A00.

3) EXPERIMENTS WITH S_{in}^{J}

In model run BJ, we assess the effects to model performance of combining the sea-state-dependent wind input term S_{in}^{J} with S_{ds}^{B}. Although S_{in}^{J} levels for strongly forced spectral components at wavenumbers higher than the peak are comparable to those of S_{in}^{Y}, they are relatively smaller for mature waves, thus providing an alternative scenario for testing the flexibility of S_{ds}^{B}. Best results using the combination of S_{ds}^{B} and S_{in}^{J} were obtained when the parameters of S_{ds}^{B} were set to $C_{ds} = 1.30 \times 10^{-2}$, $m = 1$, $n = 2$, $p_0 = 8$, and $B_r = 3.10 \times 10^{-3}$.

Results of run BJ are shown in Fig. 11. Predictions of ϵ_{**} and ν_{**} were in good agreement with the target evolution curves of KC92/94 within the valid range of their fetch-limited observations [values of percentage bias were of $O(10\%)$]. Although some residual growth was observed in the approach toward the full-development limit of A00, particularly in the calculated values of f_p, the results were considered satisfactory in terms of demonstrating that S_{ds}^{B} may also be used successfully in conjunction with S_{in}^{J}.

b. Spectral shape

Figure 12 shows the response of the spectral tail shape to using S_{ds}^{B} in association with S_{in}^{Y}, relative to the empirical parameters of B90. Predicted spectral slopes from run BYM0 approached closely the constant slope $\overline{n}_B =$

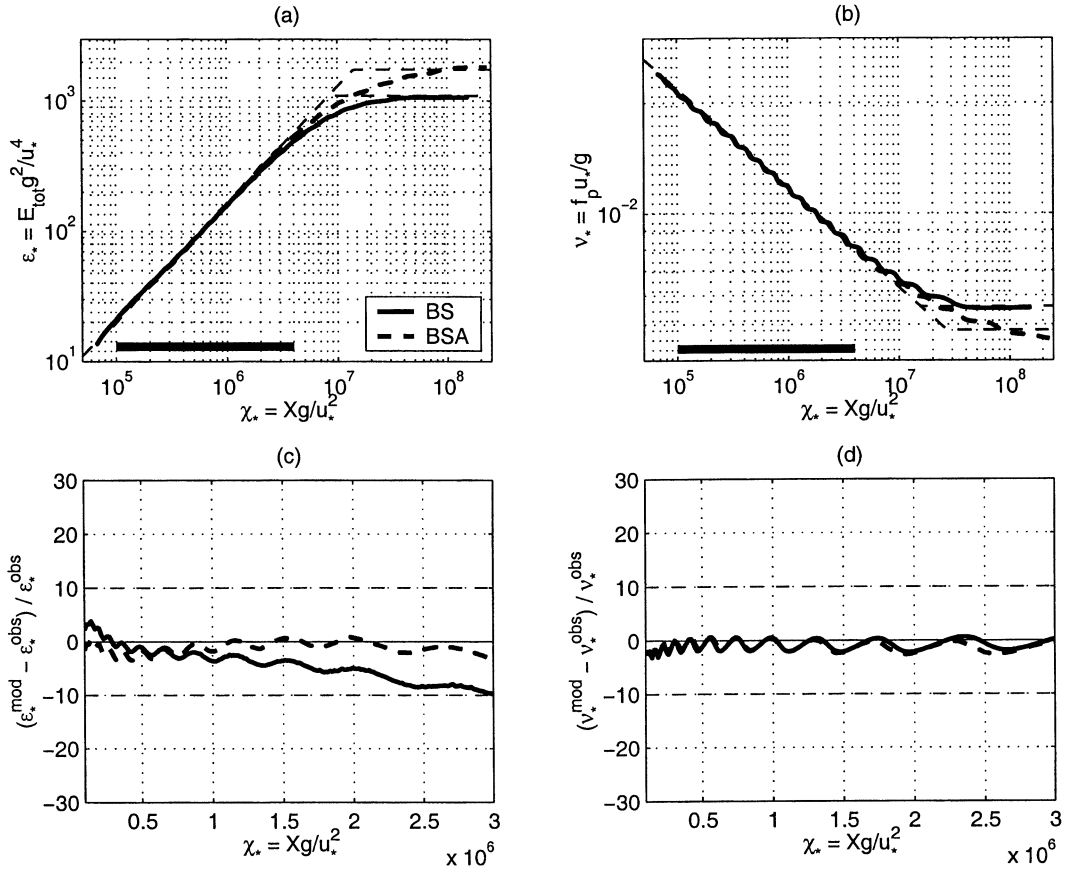

FIG. 10. Model runs BS and BSA made with S_{ds}^B and S_{in}^S. Upper diagrams show the evolution of (a) nondimensional total energy ε_* and (b) nondimensional peak frequency ν_*. The empirical KC92/94 curves are shown as dashed lines along with the full-development asymptotes of KHH and A00. (c), (d) The percentage bias of model results relative to the KC92/94 curves within the valid range of fetch-limited observations (thick horizontal lines indicated in the upper panels).

-4 inferred empirically, decreasing from approximately $\overline{n}_B = -3.80$ to $\overline{n}_B = -4.10$ with increasing wave age. Values of $\overline{\alpha}_B$ lay close to the average level of $\overline{\alpha}_B$ from B90, although not reproducing the observed trend of decreasing $\overline{\alpha}_B$ values with increasing wave age.

Computed energy density levels of the spectral tail from run BYM0 provided a relatively good match to the empirical levels of B90, as seen in Figs. 12c,d. Values of ϵ_B were approximately 1.2 times as high as $F_B(k, \theta_{wind})$ at $k = 4k_p$ within a wide range of wave development stages. At the higher relative wavenumber $k = 9k_p$, ϵ_B indicates energy densities 1.5 times as high as the empirical values in young seas and approximately 1.2 times as high in the transition to full development.

The introduction of a linear dependence of S_{ds}^B on $E_{tot}k_p^2$, investigated in run BYM1, affected positively the predicted shape of the spectral tail. Values of $\overline{n}_B$ and $\overline{\alpha}_B$ shown in Figs. 12a,b were closer to the empirical spectral tail parameters of B90 relative to run BYM0. Calculated energy densities in the wind direction slice at $4k_p$ were in good agreement with the empirical values of B90, as indicated by a relative ratio to $F_B(4k_p, \theta_{wind})$ near $\epsilon_B = 1.2$. Computed values of ϵ_B at $9k_p$ were slightly improved relative to run BYM0, now ranging from $\epsilon_B = 1.4$ at $c_p/u_* = 10$ to $\epsilon_B = 1.2$ near full development, as seen in Figs. 12a,b.

Results shown in Fig. 12 indicate that the effect of setting $m = 2$—that is, a higher nonlinear dependence of dissipation rates on $E_{tot}k_p^2$—was to increase the steepness of the predicted spectral slopes toward $\overline{n}_B \approx -4.2$, beyond the empirical values according to B90. Computed values of $\overline{\alpha}_B$ were also considerably higher than the empirical values of B90. The increase in dissipation-rate levels at short fetches, resulting from a quadratic dependence of S_{ds}^B on $E_{tot}k_p^2$, led to spectral tail energy densities that were around 20% lower than the empirical values of B90 at both $4k_p$ and $9k_p$, as seen in Figs. 12c,d.

c. Directional spreading

1) MEAN DIRECTIONAL SPREADING WIDTH

Model predictions of $\overline{\theta}$ from a selection of model runs using S_{ds}^B are shown in Fig. 13. A general feature

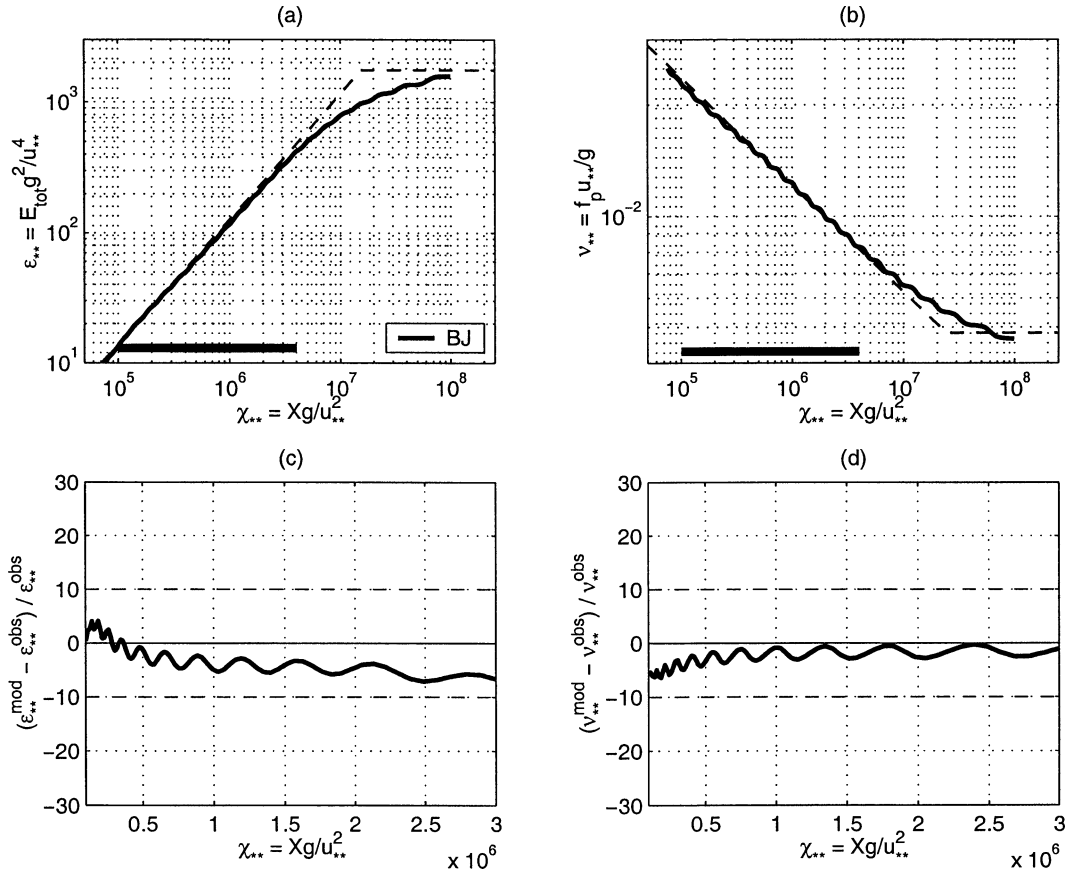

FIG. 11. Model runs made with S_{ds}^{B} and S_{in}^{J}. Upper diagrams show the evolution of (a) nondimensional total energy ε_* and (b) nondimensional peak frequency ν_*. The empirical KC92/94 curves are shown as dashed lines, along with the full-development asymptote of KHH. (c), (d) The percentage bias of model results relative to the KC92/94 curves within the valid range of fetch-limited observations (thick horizontal lines indicated in the upper panels).

of this figure, which is consistent with the empirical estimates of $\overline{\theta}$, is that all model runs predicted narrower directional spreading near the spectral peak wavenumber k_p than within the spectral tail, at $4k_p$. In all cases, however, calculated $\overline{\theta}$ were generally broader than the range of observed values at the peak and narrower at $4k_p$. Although the performance of S_{ds}^{B} in this item was relatively poorer, its trend is similar to that seen in Fig. 7 for runs made with S_{ds}^{W4}.

The upper panels in Fig. 13 show the computed $\overline{\theta}$ from model runs BYM0, BYM1, and BYM2. The major difference among these three model runs was the degree of nonlinear dependence of S_{ds}^{B} on the integral steepness parameter $E_{tot}k_p^2$, controlled by values of the exponent m. Comparisons of model results with observations of $\overline{\theta}$ indicate that changes in the exponent m had little impact on the computed directional spreading, because they were generally compensated by adjustments of the parameter $[B(k)/B_r]^{p/2}$, needed to produce a good agreement of computed spectral integrals with fetch-limited observations.

The lower panels in Fig. 13 show $\overline{\theta}$ from runs BYM1, BS, and BJ. These experiments used S_{ds}^{B} in combination with S_{in}^{Y}, S_{in}^{S}, and S_{in}^{J}, respectively. When compared with the impact of changing S_{ds}^{B} alone, (illustrated in Figs. 13a,b), results shown in Figs. 13c,d indicate that changes in the form of S_{in}—that is, changes in intensity and spectral distribution of wind input rates within the wave spectrum—have a considerable impact on the behavior of predicted directional spreading widths.

Predictions of $\overline{\theta}$ at k_p from runs BYM1 and BS, shown in Figs. 13c,d, were in agreement with observations at very low values of wave age c_p/u_* (i.e., strongly forced wind seas). Above $c_p/u_* \approx 10$, computed $\overline{\theta}(k_p)$ did not become narrower as predicted by the Babanin and Soloviev (1998) data, thus leading to a strong departure between observed and computed values. Computed mean directional widths at the spectral peak from runs BS and BYM1 were also significantly broader than the Donelan et al. (1985) data for all ranges of c_p/u_*. Model predictions of $\overline{\theta}$ at $4k_p$ from run BS were slightly broader than those from BYM1. This may have resulted from lower input rates at high wavenumbers in S_{in}^{S} relative to S_{in}^{Y}. These lower input rates at the spectral tail required

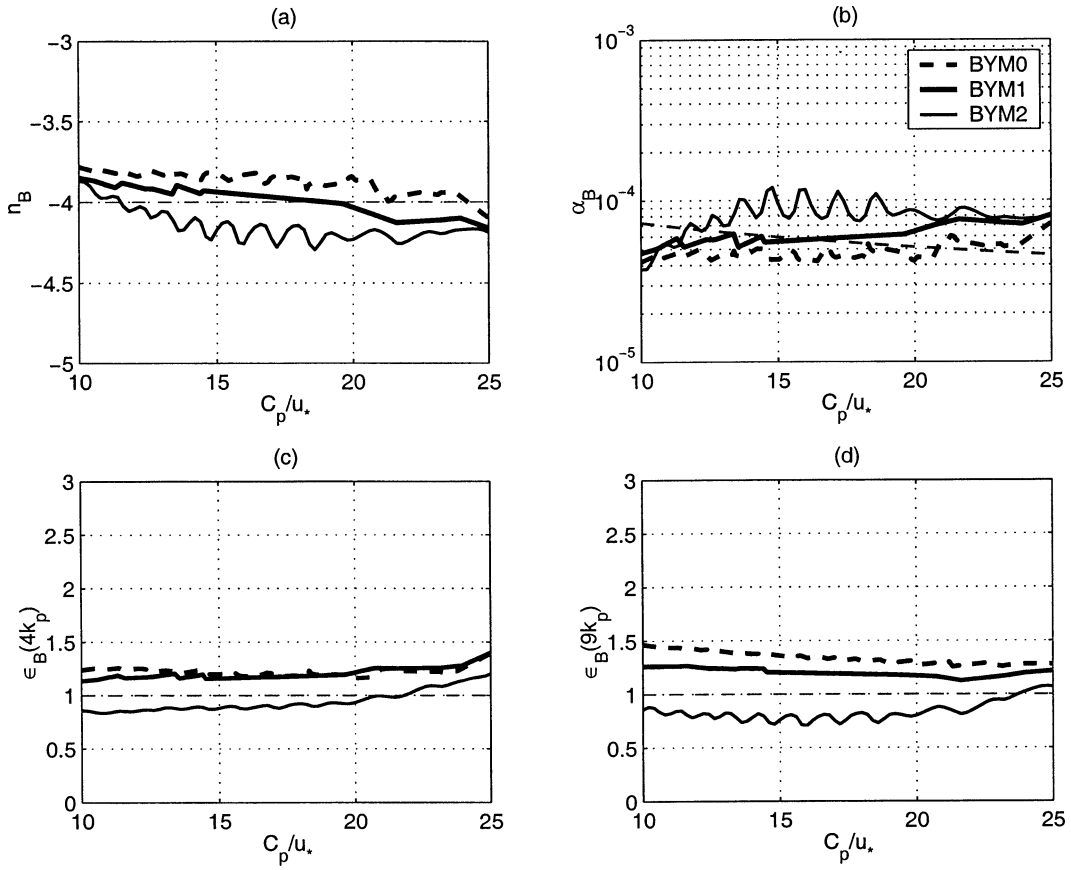

FIG. 12. Spectral tail evolution from runs BYM1, BYM0, and BYM2, made with S_{ds}^{B} vs the empirical parameters of Banner (1990): (a) average spectral tail level $\overline{\alpha}_B$ and (b) average spectral tail slope $\overline{n}_B$ and relative energy density ratio ϵ_B of the wavenumber spectral slice in the wind direction at (c) $k = 4k_p$ and (d) $k = 9k_p$.

a reduction of S_{ds}^{B} that resulted in less damping of S_{nl} for $|\theta| \gg \theta_m$, which led to predictions of $\overline{\theta}(4k_p)$ that were larger in run BS than in BYM1.

A00 shows that the nondimensional input rates prescribed by S_{in}^{J} are relatively lower than those of S_{in}^{S} and S_{in}^{Y} at the spectral peak, whereas at the spectral tail S_{in}^{J} is stronger than these two other forms of S_{in}. On average, however, the use of S_{in}^{J} resulted in enhanced input rates, particularly in earlier stages of development (i.e., young wind seas). This required a stronger S_{ds}^{B} relative to the other experiments, which resulted in a stronger damping of nonlinear S_{nl} fluxes toward $|\theta| \gg \theta_m$. As a consequence, the directional spreading of spectra generated by run BJ was narrower than in runs BYM1 and BS. Figures 13c,d show that this led to a better agreement of computed $\overline{\theta}(k)$ with the empirical relations of Donelan et al. (1985) and Babanin and Soloviev (1998) at the spectral peak but a stronger disagreement at $4k_p$.

A comparison of Figs. 7 and 13 indicates that there is no clear advantage in using either S_{ds}^{B} or S_{ds}^{W4} to provide better predictions of the mean directional spreading of computed wave spectra. Further, when compared with the analyses of BY94, these figures indicate that neither S_{ds}^{B} or S_{ds}^{W4} brought significant improvements for modeling mean directional spreading of the wave spectrum relative to S_{ds}^{W3}. These combined results, however, provide useful insight for the design of future experiments aimed at improving directional properties of simulated spectra. Because of the larger impact of the form of S_{in} on computations of $\overline{\theta}(k)$, these future experiments should include a focus on investigating the impact of alternative parameterizations of the wind input source term, such as the forms of S_{in} proposed by Tolman and Chalikov (1996), Donelan (1999), or Makin and Kudryavtsev (1999). Because these forms admit negative input rates, their impact on the predictions of $\overline{\theta}(k)$ can be much larger than the differences observed in Figs. 7 and 13.

2) HIGH-RESOLUTION DIRECTIONAL DATA

Figure 14 shows a comparison of data for the case of a mature wind sea with quasi-steady $U_{10} \approx 9.5$ m s^{-1} from Hwang et al. (2000b), with spreading angles of local spectral maxima θ_{lobe} and lobe ratios r_{lobe} calculated with the proposed saturation-based S_{ds}^{B}, using

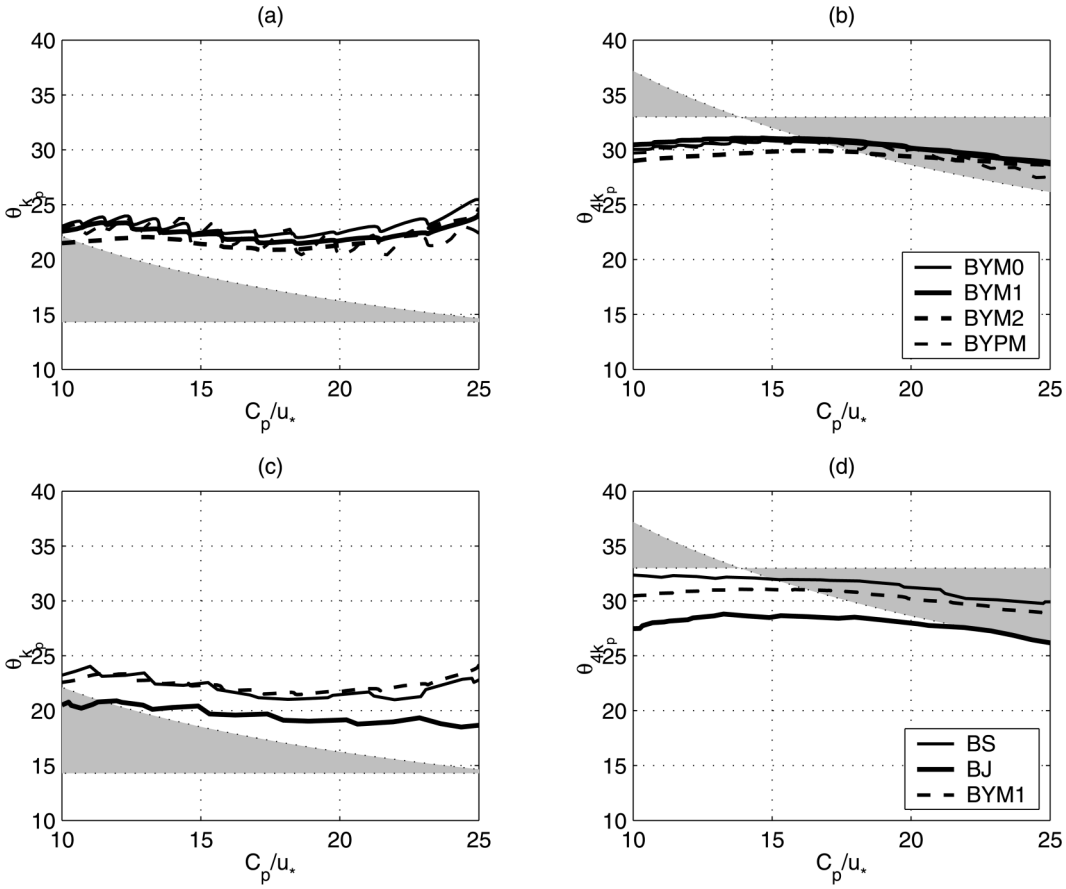

FIG. 13. Mean directional spreading width $\overline{\theta}(k)$ for runs made with S_{ds}^{B}. Validation is made against a combination of empirical mean spreading widths, resulting in the range indicated by the hatched gray area. Computed $\overline{\theta}(k)$ at k_p and at $4k_p$ are shown in the left- and right-hand panels, respectively.

the three wind-input source functions S_{in}^{Y}, S_{in}^{S} and S_{in}^{J}. This figure indicates a strong correspondence between calculated and observed θ_{lobe}, particularly in regard to the bimodal behavior. All runs made with S_{ds}^{B} closely predicted the observed unimodal behavior at the spectral peak (i.e., $k/k_p = 1$). Also, the predicted positions of directional maxima from these model runs agreed remarkably well with the observations above $4k_p$.

Results shown in Fig. 14a indicate that there was a notable sensitivity to the choice of wind input param-

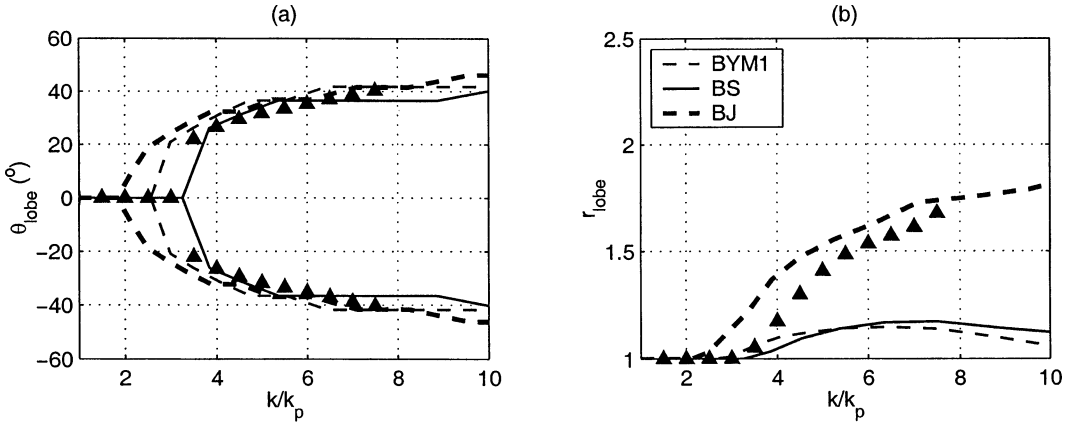

FIG. 14. Calculated (left) θ_{lobe} and (right) lobe ratios r_{lobe} from runs made with S_{ds}^{B} vs data from Hwang et al. (2000b). Measurements are indicated with triangles.

eterization in terms of predicting the point at which the spectrum makes a transition to directional bimodality. These differences were not observed in the runs with S_{ds}^{W4} because they were all made with the same form of wind-input parameterization. Figure 14b shows a comparison between calculated r_{lobe} and the empirical data of Hwang et al. (2000b). This figures confirms the importance of the specification of the form of S_{in} to modeling the directional wave energy spread. Model predictions of r_{lobe} from runs BYM1 and BS were significantly lower than the measured values, matching the S_{ds}^{W4} runs shown in Fig. 8b. Nevertheless, run BJ predicted r_{lobe} that reproduces more closely the empirical data than did all other experiments reported in our study.

d. Overview of results obtained with S_{ds}^{B}

Results presented in this section for both spectral integral quantities and high-wavenumber spectral shapes from runs made with S_{ds}^{B} show significant improvements over simulations made with S_{ds}^{W3} reported in BY94. Further, predictions of the high-wavenumber spectral shape and energy levels made with S_{ds}^{B} are also improved relative to results for S_{ds}^{W4} reported in section 4b. Our results also indicate that a persistent limitation shared by all forms of S_{ds} investigated in this study is the inability to improve model predictions of the directional spectral energy distribution.

We believe these improvements in terms of spectral integral quantities and high-wavenumber spectral shape and energy levels are due to the following properties of S_{ds}^{B}. Within the spectral peak region, S_{ds}^{B} provides a wide dynamic range of dissipation rates, which result in model predictions that are in very good agreement with empirical evolution curves of spectral integral quantities. It simultaneously provides strong dissipation levels at high wavenumbers with a relatively small dynamic range, which leads to computed spectra that reproduce closely the equilibrium range of the B90 spectral model. Other parameters in S_{ds}^{B} also contribute to producing high levels of dissipation in strongly forced young wind seas while maintaining some residual dissipation rates near full development. This general behavior apparently provides a closer match to the dynamic response of the other two source terms, S_{in} and S_{nl}, relative to S_{ds}^{W}.

A well-known feature of S_{in} is the strong reduction of input rates to the spectral peak as the wave field evolves from strongly forced to fully developed seas. Input rates within the spectral tail region, in contrast, remain comparable at any development stage. The dynamical behavior of S_{nl} is less straightforward. Numerical computations made by Resio and Perrie (1991) and Young and Van Vledder (1993) have provided deep insight on how the nonlinear fluxes within the wave spectrum change with the stage of wave growth. According to Resio and Perrie (1991), S_{nl} shows little relative change within the spectral tail at different wave evolution stages. In contrast, the nonlinear fluxes at the spectral peak are strongly affected by the spectral ''peakedness,'' which becomes less pronounced as the wave field evolves in space or time. Young and Van Vledder (1993) show that this progressive broadening of the spectral peak region leads to a reduction of nonlinear energy fluxes to the spectral peak.

Theoretical and empirical evidence thus shows that the changes of S_{in} and S_{nl} with wave growth, under active wind forcing, result in a strong dynamic response of spectral components within the spectral peak and a small variation of spectral properties at the high-wavenumber tail. In contrast, the rates of decay in S_{ds}^{W} are solely determined by the integral steepness term $(E_{tot}\bar{k}^{2}/\alpha_{PM})^{m}$, which has a constant value for all wavenumbers at any particular stage of wave growth. As a consequence, the general structure of the quasi-linear dissipation-rate source term S_{ds}^{W} is too constrained to allow the necessary differential tuning of dissipation rates needed at the spectral peak relative to the spectral tail. However, expressing S_{ds} as a function of the saturation-based term $[B(k)/B_r]^{p/2}$ in S_{ds}^{B} provides a more appropriate dynamic behavior for achieving the desired source term balance across the spectrum.

According to our results, predicted maxima of the directional wave energy spreading θ_{lobe} for mature seas from simulations made with all forms of S_{ds} tend to match the unimodal behavior at the spectral peak, making a transition to a bimodal distribution above $k/k_p \approx 3$, that was observed by Hwang et al. (2000b). Upon closer scrutiny, however, none of the forms of S_{ds} investigated was able to reproduce closely the observed variation with k/k_p of the mean directional spreading angle $\bar{\theta}$ and the directional lobe ratio r_{lobe}. We believe that the resolution of this challenging problem also involves the form of S_{in}, and this issue will be addressed in a future study.

In summary, our investigation indicates that a dissipation-rate source term nonlinearly dependent on the local wavenumber spectrum, such as the saturation-based form S_{ds}^{B}, provides a successful framework for improving wind-wave model performance in terms of predicting spectral integral quantities in fetch-limited conditions. It also shows potential for improving predictions of the shape of fetch-limited spectra. In an operational context, an initial application of S_{ds}^{B} in association with the WAM model used in the Australian region is reported by Alves et al. (2002). Their results show considerable promise for improving accuracy for hindcast waves in atmospheric conditions more complex than the idealized fetch-limited conditions considered in the present study.

7. Conclusions and recommendations

In this paper we investigate a new form of the spectral dissipation source term S_{ds} for wind-wave modeling applications. This new form of S_{ds} is based on a threshold behavior of deep-water wave-breaking onset dependent

on a mean local spectral wave steepness. It is expressed in terms of the azimuth-integrated spectral saturation, resulting in a nonlinear dependence of spectral dissipation rates on the local wave energy density spectrum. This formulation seeks to embody the concept that nonlinear wave-group modulation underlies the onset of deep-water wave breaking.

Following BY94, our investigation is based on exact nonlinear computations of fetch-limited wind-wave evolution. For reference, we present a comparative performance assessment of this saturation-based form of S_{ds} relative to dissipation-rate source terms used in the WAM model.

The main findings of our study may be summarized as follows.

1) The combination of the saturation-based S_{ds} with several commonly used parameterizations of S_{in} provides model outcomes that agree closely with spectral integral quantities derived from field observations.
2) Wavenumber spectra from most experiments made with the saturation-based S_{ds} reproduce well spectral shape parameters describing the high-wavenumber range derived from the empirical model of B90.
3) Predictions of spectral integral quantities and some properties of the high-wavenumber spectral range made with S_{ds}^{B} are generally improved relative to predictions made with the forms of S_{ds} used in the WAM model.
4) Modeled directional wave energy distributions show a unimodal behavior near the spectral peak and make a transition to a bimodal behavior above approximately 3 times the peak wavenumber, as observed by Hwang et al. (2000b). However, quantitative measures of these directional spreading properties, particularly the variation with k/k_p of the mean spreading angle and lobe ratio, do not conform closely to the available observations for any of the variants of S_{ds} that were investigated.

The present investigation suggests that forms of S_{ds} nonlinearly dependent on the local wave spectral density, such as the saturation-based form S_{ds}^{B}, provide a physically based, flexible framework for further improvements of wind-wave model performance.

Our results indicate that future developments of alternative forms of S_{ds} should include

1) implementing a breaking-threshold saturation level based on observed values, as such data become available;
2) refining the breaking-threshold saturation level to reflect the directional properties of the wave spectrum;
3) investigating the effect on model predictions of directional wave energy spread of refined parameterizations of S_{in}, including loss of wave energy to slow/opposing winds, such as those proposed by Tolman and Chalikov (1996), Donelan (1999), and/or Makin and Kudryavtsev (1999);
4) investigating the effect on model performance of improved or alternative parameterizations of the nonlinear interactions source term S_{nl};
5) assessing the performance of alternative parameterizations of source terms under a wider range of wave-generation conditions, using higher-quality forcing winds measured in the field; and
6) investigating the impact on model outcomes of algorithms that quantify the dynamic coupling between winds and waves.

Acknowledgments. We are very grateful for the suggestions provided by Professor Ian R. Young. The support of the following organizations is gratefully acknowledged: Conselho Nacional de Desenvolvimento Cientifico e Tecnologico (CNPq), Brazil, through the Ph.D. scholarship GDE 200.241/96-6 for JHGMA, and the Australian Research Council and U.S. Office of Naval Research for MLB. We also acknowledge the operational support of the Schools of Mathematics and Civil Engineering/ADFA of The University of New South Wales and the Faculty of Engineering, Mathematics and Computer Sciences of The University of Adelaide.

REFERENCES

Agrawal, Y. C., E. A. Terray, M. A. Donelan, P. A. Hwang, A. J. Williams III, W. M. Drennan, K. K. Kahma, and S. A. Kitaigorodskii, 1992: Enhanced dissipation of kinetic energy beneath surface waves. *Nature,* **359,** 219–220.

Alves, J. H. G. M., 2000: A saturation-dependent dissipation source function for wind-wave modelling applications. Ph.D. thesis, The University of New South Wales, Sydney, Australia, 237 pp.

——, D. A. Greenslade, and M. L. Banner, 2002: Impact of a saturation-dependent dissipation function on wave hindcasts in the Australian region. *Global Atmos. Ocean Syst.,* **8,** 239–267.

Babanin, A. V., and Y. P. Soloviev, 1998: Variability of directional spectra of wind-generated waves, studied by means of wave staff arrays. *Mar. Freshwater Res.,* **49,** 89–101.

Banner, M. L., 1990: Equilibrium spectra of wind waves. *J. Phys. Oceanogr.,* **20,** 966–984.

——, and I. R. Young, 1994: Modeling spectral dissipation in the evolution of wind waves. Part I: Assessment of existing model performance. *J. Phys. Oceanogr.,* **24,** 1550–1570.

——, I. S. F. Jones, and J. C. Trinder, 1989: Wavenumber spectra of short gravity waves. *J. Fluid Mech.,* **198,** 321–344.

——, A. V. Babanin, and I. R. Young, 2000: Breaking probability for dominant waves on the sea surface. *J. Phys. Oceanogr.,* **30,** 3145–3160.

Booij, N., R. C. Ris, and L. H. Holthuijsen, 1999: A third generation wave model for coastal regions. Part 1. Model description and validation. *J. Geophys. Res.,* **104,** 7649–7666.

Chen, G., and S. Belcher, 2000: Effects of long waves on wind-generated waves. *J. Phys. Oceanogr.,* **30,** 2246–2256.

Chu, G. S., S. R. Long, and O. M. Phillips, 1992: Measurements of the interaction of wave groups with shorter wind-generated waves. *J. Fluid Mech.,* **245,** 191–210.

Dold, J. W., and D. H. Peregrine, 1986: Water-wave modulation. *20th Int. Conf. on Coastal Engineering,* Taipei, Taiwan, ASCE, 163–176.

Donelan, M. A., 1982: The dependence of the aerodynamic drag coefficient on wave parameters. Preprints, *First Int. Conf. Meteorology and Air–Sea Interaction of the Coastal Zone*, The Hague, Netherlands, Amer. Meteor. Soc., 381–387.
——, 1984: Attenuation of laboratory swell in adverse wind. National Water Research Institute Rep., Burlington, ON, Canada, 26 pp.
——, 1996: Air–water exchange processes. *Physical Processes in Lakes and Oceans*, J. Imberger, Ed., *Coastal and Estuarine Studies*, Vol. 54, Amer. Geophys. Union, 19–36.
——, 1999: Wind-induced growth and attenuation of laboratory waves. *Wind-over-Wave Couplings: Perspectives and Prospects*, S. G. Sajjadi et al., Eds., University of Salford, 183–194.
——, and W. J. Pierson, 1987: Radar scattering and equilibrium ranges in wind-generated waves with application to scatterometry. *J. Geophys. Res.*, **92,** 4971–5029.
——, and Y. Yuan, 1994: Wave dissipation by surface processes. *Dynamics and Modelling of Wind Waves*, G. J. Komen et al., Eds., Cambridge University Press, 143–155.
——, M. S. Longuet-Higgins, and J. S. Turner, 1972: Periodicity in whitecaps. *Nature*, **239,** 449–451.
——, J. Hamilton, and W. H. Hui, 1985: Directional spectra of wind-generated waves. *Philos. Trans. Roy. Soc. London*, **A315,** 509–562.
——, F. W. Dobson, S. D. Smith, and R. J. Anderson, 1993: On the dependence of sea surface roughness on wave development. *J. Phys. Oceanogr.*, **23,** 2143–2149.
Drennan, W. M., M. A. Donelan, E. A. Terray, and K. B. Katsaros, 1997: On waves, oceanic turbulence, and their interaction. *Geophysica*, **33,** 17–27.
Gemmrich, J. R., and D. M. Farmer, 1999: Near-surface turbulence and thermal structure in a wind-driven sea. *J. Phys. Oceanogr.*, **29,** 480–499.
Green, T., H. Medwin, and J. E. Paquin, 1972: Measurements of surface wave decay due to underwater turbulence. *Nature*, **237,** 115.
Günther, H., S. Hasselmann, and P. A. E. M. Janssen, 1992: The WAM model Cycle 4. Tech. Rep. 4, German Climate Research Center, DKRZ, Hamburg, Germany, 102 pp.
Hasselmann, K., 1962: On the nonlinear energy transfer in a gravity-wave spectrum. Part 1: General theory. *J. Fluid Mech.*, **12,** 481–500.
——, 1974: On the spectral dissipation of ocean waves due to whitecapping. *Bound.-Layer Meteor.*, **6,** 107–127.
——, and Coauthors, 1973: Measurements of wind-wave growth and swell decay during the joint North Sea wave project (JONSWAP). *Dtsch. Hydrogr. Z.*, **8A** (Suppl.), 1–95.
Hersbach, H., 1998: Application of the adjoint of the WAM model to inverse wave modeling. *J. Geophys. Res.*, **103** (C5), 10 469–10 487.
Holthuijsen, L. H., and T. H. C. Herbers, 1986: Statistics of breaking waves observed as whitecaps in the open sea. *J. Phys. Oceanogr.*, **16,** 290–297.
Hwang, P. A., D. Wang, E. Walsh, W. Krabill, and R. Swift, 2000a: Airborne measurements of the wavenumber spectra of ocean surface waves. Part I: Spectral slope and dimensionless spectral coefficient. *J. Phys. Oceanogr.*, **30,** 2753–2767.
——, ——, ——, ——, and ——, 2000b: Airborne measurements of the wavenumber spectra of ocean surface waves. Part II: Directional distribution. *J. Phys. Oceanogr.*, **30,** 2768–2787.
Janssen, P. A. E. M., 1991: Quasi-linear theory of wind wave generation applied to wave forecasting. *J. Phys. Oceanogr.*, **21,** 1631–1642.
——, 1994: Wave growth by wind. *Dynamics and Modelling of Wind Waves*, G. J. Komen et al., Eds., Cambridge University Press, 71–112.
Kahma, K., and C. J. Calkoen, 1992: Reconciling discrepancies in the observed growth of wind-generated waves. *J. Phys. Oceanogr.*, **22,** 1389–1405.
——, and ——, 1994: Growth curve observations. *Dynamics and Modelling of Wind Waves*, G. J. Komen et al., Eds., Cambridge University Press, 143–155.
Kitaigorodskii, S. A., 1983: On the theory of the equilibrium range in the spectrum ofwind-generated gravity waves. *J. Phys. Oceanogr.*, **13,** 816–827.
Kolaini, A. R., and M. P. Tulin, 1995: Laboratory measurements of breaking inception and post-breaking dynamics of steep short-crested waves. *Int. J. Offshore Polar Eng.*, **5,** 212–218.
Komen, G. J., S. Hasselmann, and K. Hasselmann, 1984: On the existence of a fully developed wind-sea spectrum. *J. Phys. Oceanogr.*, **14,** 1271–1285.
——, L. Cavaleri, M. Donelan, K. Hasselmann, S. Hasselmann, and P. A. E. M. Janssen, 1994: *Dynamics and Modelling of Ocean Waves.* Cambridge University Press, 532 pp.
Lewis, A. W., and R. N. Allos, 1990: JONSWAP's parameters: Sorting out inconsistencies. *Ocean Eng.*, **17,** 409–415.
Makin, V. K., and V. N. Kudryavtsev, 1999: Coupled sea surface-atmosphere model. Part 1. Wind over waves coupling. *J. Geophys. Res.*, **104,** 7613–7623.
——, ——, and C. Mastenbroek: 1995: Drag of the sea surface. *Bound.-Layer Meteor.*, **73,** 159–182.
Meza, E., J. Zhang, and R. J. Seymour, 2000: Free-wave energy dissipation in experimental breaking waves. *J. Phys. Oceanogr.*, **30,** 2404–2418.
Mitsuyasu, H., 1966: Interactions between water waves and wind. Research Institute of Applied Mechanics Rep. 14, Kyushu University, 67–88.
Nepf, H. M., C. H. Wu, and E. S. Chan, 1998: A comparison of two- and three-dimensional wave breaking. *J. Phys. Oceanogr.*, **28,** 1496–1510.
Phillips, O. M., 1984: On the response of short ocean wave components at a fixed wavenumber to ocean current variations. *J. Phys. Oceanogr.*, **14,** 1425–1433.
——, 1985: Spectral and statistical properties of the equilibrium range in wind-generated gravity waves. *J. Fluid Mech.*, **156,** 505–531.
——, and M. L. Banner, 1974: Wave breaking in the presence of wind drift and swell. *J. Fluid Mech.*, **66,** 625–640.
Pierson, W. J., and L. Moskowitz, 1964: A proposed spectral form for fully-developed wind seas based on the similarity theory of A. A. Kitaigorodskii. *J. Geophys. Res.*, **69,** 5181–5190.
Plant, W. J., 1982: A relationship between wind stress and wave slope. *J. Geophys. Res.*, **87,** 1961–1967.
Rapp, R. J., and W. K. Melville, 1990: Laboratory measurements of deep-water breaking waves. *Philos. Trans. Roy. Soc. London*, **A331,** 735–800.
Resio, D., and W. Perrie, 1991: A numerical study of nonlinear energy fluxes due to wave-wave interactions. Part 1. Methodology and basic results. *J. Fluid Mech.*, **223,** 603–629.
Schneggenburger, C., H. Gunther, and W. Rosenthal, 2000: Spectral wave modelling with nonlinear dissipation: Validation and applications in a coastal tidal environment. *Coastal Eng.*, **41,** 201–235.
She, K., C. A. Greated, and W. J. Easson, 1997: Experimental study of three-dimensional breaking wave kinematics. *Appl. Ocean Res.*, **19,** 329–343.
Smith, S., and Coauthors, 1992: Sea surface wind stress and drag coefficients. *Bound.-Layer Meteor.*, **60,** 109–142.
Snyder, R. L., F. W. Dobson, J. A. Elliot, and R. B. Long, 1981: Array measurements of atmospheric pressure fluctuations above surface gravity waves. *J. Fluid Mech.*, **102,** 1–59.
Song, J. B., and M. L. Banner, 2002: On determining the onset and strength of breaking for deep water waves. Part I: Unforced irrotational wave groups. *J. Phys. Oceanogr.*, **32,** 2541–2558.
Thais, L., and J. Magnaudet, 1996: Turbulent structure beneath surface gravity waves sheared by the wind. *J. Fluid Mech.*, **328,** 313–344.
Tolman, H. L., 1999: User manual and system documentation of WAVEWATCH-III, version 1.18. NCEP/NOAA Tech. Note 116, 110 pp.

——, and D. Chalikov, 1996: Source terms in a third-generation wind wave model. *J. Phys. Oceanogr.*, **26,** 2497–2518.

Tracy, B. A., and D. T. Resio, 1982: Theory and calculation of the nonlinear energy transfer between sea waves in deep water. WIS Rep. 11, U.S. Army Engineer Waterways Experiment Station, 48 pp.

Tulin, M. P., and T. Waseda, 1999: Laboratory observations of wave group evolution, including breaking effects. *J. Fluid Mech.*, 197–232.

Webb, D. J., 1978: Nonlinear transfers between sea waves. *Deep-Sea Res.*, **25,** 279–298.

Yan, L., 1987: An improved wind input source term for third generation ocean wave modelling. Royal Netherlands Meteorological Institute Scientific Rep. WR-87-8, 10 pp.

Young, I. R., 1995: The determination of confidence limits associated with estimates of the spectral peak frequency. *Ocean Eng.*, **22,** 669–686.

——, and G. P. Van Vledder, 1993: A review of the central role of nonlinear interactions in wind-wave evolution. *Philos. Trans. Roy. Soc. London*, **342,** 505–524.

Zakharov, V. E., and N. N. Filonenko, 1967: Energy spectrum for stochastic oscillations of the surface of a liquid. *Sov. Phys. Dokl.*, **11,** 881–883.